

# Lawrence Berkeley National Laboratory

## LBL Publications

### Title

Joint Time-Lapse Acquisition and Inversion of Passive Seismic and Magnetotelluric Data for Monitoring Reservoir Processes at The Geysers Geothermal Field

### Permalink

<https://escholarship.org/uc/item/72h9t80n>

### Author

Gritto, Roland

### Publication Date

2024-06-10

Peer reviewed



**CALIFORNIA  
ENERGY COMMISSION**



**CALIFORNIA  
NATURAL  
RESOURCES  
AGENCY**

**ENERGY RESEARCH AND DEVELOPMENT DIVISION  
FINAL PROJECT REPORT**

**Joint Time-Lapse Acquisition and  
Inversion of Passive Seismic and  
Magnetotelluric Data for Monitoring  
Reservoir Processes at The Geysers  
Geothermal Field**

**June 2024 | CEC-500-2024-075**



**PREPARED BY:**

Dr. Roland Gritto  
EMR Solutions and Technology  
**Primary Author**

Katherine Greenwald, Chuck Gentry  
**Project Manager**  
**California Energy Commission**

**Agreement Number:** EPC-19-019

Kevin Uy  
**Branch Manager**  
**ENERGY SUPPLY BRANCH**

Jonah Steinbuck, Ph.D.  
**Director**  
**ENERGY RESEARCH AND DEVELOPMENT DIVISION**

Drew Bohan  
**Executive Director**

**DISCLAIMER**

**This report was prepared as the result of work sponsored by the California Energy Commission (CEC). It does not necessarily represent the views of the CEC, its employees, or the State of California. The CEC, the State of California, its employees, contractors, and subcontractors make no warranty, express or implied, and assume no legal liability for the information in this report; nor does any party represent that the uses of this information will not infringe upon privately owned rights. This report has not been approved or disapproved by the CEC, nor has the California Energy Commission passed upon the accuracy or adequacy of the information in this report.**

## **ACKNOWLEDGEMENTS**

The authors acknowledge the California Energy Commission (CEC) for financial assistance under contract EPC-19-019. The authors would like to thank Chuck Gentry and Katherine Greenwald (CEC contract managers) for their continued support during the project. The authors are grateful to the members of the Technical Advisory Committee, Professor Douglas Dreger, Dr. Randall Mackie, and Craig Hartline, who provided technical guidance throughout the course of the project. The authors are also indebted to Calpine Corporation for access to The Geysers geothermal field. Finally, the authors would like to extend special thanks to Craig Hartline for providing reservoir data and numerous fruitful discussions on reservoir properties and on the interpretation of the geophysical data as they relate to reservoir operations.

## PREFACE

The California Energy Commission's (CEC) Energy Research and Development Division supports energy research and development programs to spur innovation in energy efficiency, renewable energy and advanced clean generation, energy-related environmental protection, energy transmission, and distribution and transportation.

In 2012, the Electric Program Investment Charge (EPIC) was established by the California Public Utilities Commission to fund public investments in research to create and advance new energy solutions, foster regional innovation, and bring ideas from the lab to the marketplace. The EPIC Program is funded by California utility customers under the auspices of the California Public Utilities Commission. The CEC and the state's three largest investor-owned utilities—Pacific Gas and Electric Company, San Diego Gas and Electric Company, and Southern California Edison Company—were selected to administer the EPIC funds and advance novel technologies, tools, and strategies that provide benefits to their electric ratepayers.

The CEC is committed to ensuring public participation in its research and development programs that promote greater reliability, lower costs, and increase safety for the California electric ratepayer and include:

- Providing societal benefits.
- Reducing greenhouse gas emission in the electricity sector at the lowest possible cost.
- Supporting California's loading order to meet energy needs first with energy efficiency and demand response, next with renewable energy (distributed generation and utility scale), and finally with clean, conventional electricity supply.
- Supporting low-emission vehicles and transportation.
- Providing economic development.
- Using ratepayer funds efficiently.

For more information about the Energy Research and Development Division, please visit the [CEC's research website \(www.energy.ca.gov/research/\)](http://www.energy.ca.gov/research/) or contact the Energy Research and Development Division at [ERDD@energy.ca.gov](mailto:ERDD@energy.ca.gov).

# ABSTRACT

This project successfully implemented an approach to jointly image time-lapse changes in water and steam concentrations and subsurface flow in a geothermal reservoir, using data from small earthquakes and magnetotelluric observations. The project advanced the technology by imaging time-lapse changes of the two data sets, based on different physical properties, for the first time. The project demonstrated this technology at The Geysers geothermal field in Northern California over an area of approximately 75 square kilometers, where seismic and magnetotelluric data were collected over several years. The project team collected seismic data from over 280,000 earthquakes and collected three magnetotelluric surveys to generate images of water and steam volumes as well as flow paths and barriers in the geothermal reservoir. Correlation of the geophysical images with known water injection and steam production volumes allowed the team to calibrate the data and to gain confidence in the results, which can now be applied throughout the reservoir, where borehole data are unavailable. The results of the joint imaging, together with reservoir data derived from observations in boreholes, allow interpretation of the images to identify water and steam saturated zones, as well as fluid pathways and barriers. This information allows the reservoir operator to improve its drilling program by minimizing drilling of unsuccessful wells, resulting in reduced costs and lower electricity rates for California ratepayers.

**Keywords:** Joint-inversion of multiple-physics data, induced seismicity, MT data, large-scale characterization of a geothermal reservoir, delineation of injection and production zones

Please use the following citation for this report:

Gritto, Roland, Evan S. Um, Jared Peacock, Steve P. Jarpe, Craig Ulrich, Craig S. Hartline, and David L. Alumbaugh. 2024. *Joint Time-Lapse Acquisition and Inversion of Passive Seismic and Magnetotelluric Data for Monitoring Reservoir Processes at The Geysers Geothermal Field*. California Energy Commission. Publication Number: CEC-500-2024-075

# TABLE OF CONTENTS

Acknowledgements .....	i
Preface .....	ii
Abstract .....	iii
Executive Summary .....	1
Background .....	1
Project Purpose and Approach .....	1
Key Results .....	2
Knowledge Transfer and Next Steps .....	2
CHAPTER 1: Introduction .....	4
CHAPTER 2: Project Approach .....	7
Passive Seismic Data Acquisition and Processing .....	8
Magnetotelluric Data Acquisition and Processing .....	10
Joint Inversion of Multiphysics Data .....	12
Appraising Geophysical Data Through Geothermal Reservoir Model .....	15
CHAPTER 3: Results .....	17
Passive Seismic Data Acquisition and Processing .....	17
Magnetotelluric Data Acquisition and Processing .....	20
Joint Inversion of Multiphysics Data .....	24
Single-Physics Inversion .....	25
Multiple-Physics Inversion .....	26
Time-Lapse Multi-Physics Inversion .....	27
Appraising Geophysical Data Through Geothermal Reservoir Model .....	29
Appraising Spatio-temporal Vp/Vs Results .....	29
Appraising Spatio-temporal Vp/Vs and Electrical Conductivity Results .....	33
CHAPTER 4: Conclusion .....	35
Glossary and List of Acronyms .....	37
References .....	39
Project Deliverables .....	43
APPENDIX A: Passive Seismic Imaging .....	A-1
APPENDIX B: Time-lapse Joint Inversion .....	B-1
APPENDIX C: Geophysical Data Acquisition .....	C-1

## LIST OF FIGURES

Figure 1: Cross Sections Through The Geysers Geothermal Reservoir from SW to NE .....	6
Figure 2: Map of The Geysers With Locations of Seismic and MT Stations.....	8
Figure 3: Seismic Traces With Detections of Seismic Phase Arrival by PhaseNet .....	9
Figure 4: Map With MT Sites of the Annual Surveys.....	11
Figure 5: Geometry of an MT Station.....	12
Figure 6: The Joint Inversion Workflow .....	14
Figure 7: The Geysers 3D Structural Reservoir Model.....	16
Figure 8: Horizontal Slices of Temporal Changes in Vp/Vs .....	18
Figure 9: Vertical Cross Sections of Temporal Changes in Vp/Vs .....	19
Figure 10: Residual Phase Tensor Maps for Periods of 10 Seconds and 20 Seconds.....	20
Figure 11: Residual Phase Tensor Maps for Periods of 30 Seconds and 50 Seconds.....	21
Figure 12: Residual Phase Tensor for Period of 10 Seconds on Map and in Cross-Sectional View .....	23
Figure 13: Iso-Surface Plot With Change in Electrical Conductivity Between 2017 and 2021.....	24
Figure 14: Map With the Location of Seismic and MT Stations and Two Profiles .....	25
Figure 15: Cross Sections of Vp/Vs and Electrical Conductivity After Single Inversion.....	26
Figure 16: Cross Sections of Vp/Vs and Electrical Conductivity After Joint Inversion.....	27
Figure 17: Cross Sections of Electrical Conductivity and Vp/Vs After Joint Inversion.....	28
Figure 18: Map of The Geysers With Water Injectors and Temporal Changes in Vp/Vs.....	30
Figure 19: Map of The Geysers With Water Injectors and Temporal Changes in Vp/Vs.....	31
Figure 20: Vertical View of Temporal Changes in Vp/Vs in Vicinity of the Prati-15 in the Northwest Geysers.....	32
Figure 21: Temporal Changes of Vp/Vs for Steam Producer Prati-31 in the Northwest Geysers .....	33
Figure 22: Temporal Changes in Vp/Vs and Electrical Conductivity for Water Injector Prati-32 in the Northwest Geysers.....	34
Figure 23: Temporal Changes in Vp/Vs and Electrical Conductivity for Water Injector CMHC2_RD1 in the Central Geysers .....	34
Figure A-1: Map With Co-located Earthquakes From 2018.2019 and 2020 .....	A-2



Figure A-2: Histogram of the Separation Distance Between Selected Earthquakes in 2018.2019 and 2020.....	A-3
Figure A-3: Horizontal Slices of Temporal Changes in Vp/Vs .....	A-4
Figure A-4: Vertical Cross Sections of Temporal Changes in Vp/Vs .....	A-5
Figure B-1: Cross Sections of Vp/Vs for Years 2021 and 2023 After Single Inversion .....	B-2
Figure B-2: Cross Sections of Electrical Conductivity for Years 2021 and 2023 After Single Inversion .....	B-2
Figure C-1: Temporary Seismic Station Components .....	C-2
Figure C-2: Permanent Seismic Station at The Geysers Geothermal Reservoir .....	C-3
Figure C-3: Temporary Seismic Station at The Geysers Geothermal Reservoir .....	C-4
Figure C-4: Damaged Temporary Seismic Stations at The Geysers Reservoir .....	C-5
Figure C-5: Schematic of a Basic Magnetotelluric Field Station .....	C-6
Figure C-6: Magnetic Field Sensor and Electrodes.....	C-7
Figure C-7: Magnetotelluric Field Equipment and Data Transfer to a Computer .....	C-7

## **LIST OF TABLES**

Table C-1: Physical Properties of Temporary Seismic Station .....	C-2
---	-----

# Executive Summary

---

## Background

California Senate Bill 100 established a statewide goal of 60 percent electricity generation from renewable sources by 2030. Continued growth of California's broad portfolio of renewable energy, including geothermal, is required to achieve the goals of SB 100. However, a major barrier to achieving the state's mandated renewable electricity targets is that fluctuating resources like wind and solar require complementary resources and strategies to ensure grid reliability. Geothermal energy, a virtually untapped energy resource derived from the earth's heat, is a key complementary resource that is independent of external weather conditions and provides clean, renewable power around the clock, emits little or no greenhouse gases, and takes a very small environmental footprint to develop.

Over the years, state and federal agencies have helped develop, demonstrate, and install innovative technologies to stimulate the growth of the geothermal industry within the renewable energy sector and encourage quick adoption of these technologies by the public and private sectors. Geothermal energy resource development relies on boreholes that tap the earth's heat. This heat is brought to the surface in the form of hot water or steam and drives turbines that generate electricity.

Geothermal boreholes can cost as much as \$8.5 million, and providing reliable information on the drilling target at depth reduces the risk of a dry or unsuccessful well. However, determining exactly where to place geothermal wells is not a trivial issue. To address this concern, this project developed technology that provides high-resolution images of the structure of the earth's crust in the geothermal reservoir, including the location of water, steam, and flow barriers to help geothermal operators decide where to successfully situate boreholes. The project employed two remote sensing techniques based on disparate geophysical data that image the same properties in the reservoir (water, steam, and flow barriers such as faults). The techniques comprise micro-seismic imaging, which transforms ground vibrations from earthquakes into images of the reservoir structure and magnetotelluric (MT) imaging, which uses electromagnetic fields in the earth's atmosphere to image the same properties at depth. Using the different data jointly and generating images of the subsurface properties produces results that increase the reliability of the location and of the physical properties of the reservoir parameters. The developed technology generates results with the level of detail required for reliable and accurate placement of boreholes.

## Project Purpose and Approach

The goal of the current project included the development of geophysical imaging techniques using seismic and MT data to jointly image structural features and dynamic properties of the reservoir to support energy generation at The Geysers geothermal field. The technical advancements of this project are provided via: (1) the monitoring of time-lapse changes in both seismic velocity and electrical conductivity that are occurring in the reservoir due to water injection and steam production; and (2) the joint inversion of the multi-physics (seismic and

MT) data, which can provide images of the reservoir structure with higher confidence than can either of the data sets by themselves. Ultimately, these images can be used for better estimates of rock properties and spatial distribution of steam and water at depth, for more accurate reservoir modeling and monitoring and for more accurate placement of production wells.

## **Key Results**

The demonstration of the technology in the field proved successful. The metrics to demonstrate success included spatio-temporal correlation with a three-dimensional (3D) reservoir model that was based on measurements and observations in hundreds of boreholes throughout The Geysers steam field. The passive seismic data acquisition and processing detected and analyzed more than 220,000 earthquakes that were recorded over a period of five years. The 3D imaging resulting from seismic data correlated with the locations of steam and water in the geothermal reservoir and can be used to improve the understanding of the geothermal resource. Three repeat MT surveys were conducted during the project. Processing the MT data generated 3D images of electrical conductivity that also correlated spatially with the locations of steam and water in the reservoir. Information contained in The Geysers 3D reservoir model corroborated most of the results of the joint seismic and MT imaging. The results yielded high-resolution images of the complex structure of the reservoir that showed regions with high concentrations of steam and water, and flow barriers in the form of faults. While regions with high steam concentrations are targets for future production wells, knowing the location of water-saturated zones is useful to drill complementary injection wells to optimally distribute water in the reservoir.

The results of the project add confidence in the development of the 3D reservoir model, which forms the basis for reservoir management, such as well planning and siting. Knowing the spatial distribution of water and steam reduces the danger of drilling dry holes. Drilling costs of boreholes range from \$7.0 million for wells 8,500 feet in length to \$8.3 million for wells 10,000 feet in length. In the current case, the cost savings for the California rate payer can be substantial, considering that the project covered about 80 percent of The Geysers steam field with several hundred boreholes.

The results of the project also support the continued management of the resource at The Geysers, assuring the sustained viability of the resource in the future. Geothermal energy is clean, has a small environmental footprint, and is available 24 hours per day. It is independent of sunlight or wind speed, as in the case of solar installations or wind turbines. Therefore, geothermal energy adds a reliable source to California's green energy portfolio.

## **Knowledge Transfer and Next Steps**

The research team reported project results at scientific conferences and in scientific journals. During the project, four papers were presented at the Stanford Geothermal Workshop, while two papers were published in peer-reviewed journals.

The immediate results of the project are being used by Calpine Corporation (Calpine) to inform its drilling program in the study area and to manage the viability of the resource. To that effect, Calpine incorporated the derived 3D models of seismic and electric properties into its

3D reservoir model and will use those models to guide drilling operations at present and in the future. At the writing of this report, Calpine is drilling new wells and plans the reopening and deepening of abandoned wells to improve production in the northwestern region of the reservoir.

Mid-term target markets include geothermal reservoirs in California, including the Coso and Salton Sea geothermal fields. The application of the developed technique to other geothermal reservoirs is straightforward. Because the seismic method is passive, the cost of data acquisition is low and automated data processing techniques are readily available. Furthermore, MT surveys can be acquired by a small crew in one to two weeks, depending on the size of the reservoir, which minimizes acquisition cost. As such, the technology can be applied as long as sufficiently high rates of natural or induced seismicity through water injection is observed. It is noted that, in regions where the rate of seismicity is lower than at The Geysers, MT data might help to provide higher resolution.

Long-term markets for this technology include geothermal reservoirs outside of California, such as new developments in Cascadia (northwestern United States), Nevada, Idaho, Utah, and Hawaii, where planned enhanced geothermal systems are expected to generate induced seismicity. Additionally, international markets may include geothermally productive regions such as Iceland, Turkey, Taiwan, the Philippines, Indonesia, and New Zealand.

The lower resolution of MT data compared to seismic data limits the utility of the resulting electric conductivity images to increasing the confidence in the seismic results, rather than improving the resolution of the joint multi-physics images. This can be improved by jointly acquiring and inverting MT data and controlled source electromagnetic (CSEM) data. CSEM data can be acquired using a limited number of grounded electric dipole sources, keeping data acquisition costs low. The joint inversion of MT and CSEM data not only ensures imaging depths that effectively cover geothermal reservoirs but also enhances resolution. Thus, the combination of passive seismic, MT, and CSEM imaging should be investigated in a future study.

# CHAPTER 1:

## Introduction

---

In contrast to weather-dependent renewable resources such as solar and wind, geothermal energy is a virtually untapped energy resource derived from the earth's heat that provides clean, renewable power around the clock, emits little or no greenhouse gases, and takes a very small environmental footprint to develop. By developing, demonstrating, and deploying innovative technologies, the United States Department of Energy (U.S. DOE) Geothermal Technology Office's (GTO) efforts are helping to stimulate the growth of the geothermal industry within the renewable energy sector and encouraging quick adoption of technologies by the public and private sectors.

The California Energy Commission (CEC) supports similar goals with its portfolio of geothermal-related research projects in California that are aimed at stimulating geothermal growth, reducing the cost of geothermally generated electricity, and helping the California rate payer with lower electricity rates.

The technology, developed under the current project, is aimed at helping to understand the geological complexity of The Geysers geothermal reservoir in the Mayacamas Mountains in Northern California. The Geysers are the world's largest geothermal power plant with an electricity generation capacity of approximately 800 megawatts (MW). Geothermal electricity is generated by injecting water in boreholes deep into the hot volcanic rock and retrieving steam from different boreholes to power generators to produce electricity. Knowing the distribution of water and steam in the heterogeneous reservoir is paramount for operators to evaluate their reservoir management and to better understand their use of the resource including water injection, steam production, and well-planning operations. This knowledge will reduce the cost of operations and consequently the cost of generated electricity for California ratepayers. However, knowing the exact location to site geothermal wells is not a trivial issue. Most information about the state of the geothermal reservoir is derived from observations in numerous boreholes that have been drilled into The Geysers reservoir. These observations represent point measurements of the three-dimensional (3D) reservoir that is characterized by a high degree of heterogeneity. What are needed are remote sensing methods that can image the heterogeneity in the reservoir in three dimensions with specific emphasis on the spatial distribution of water and steam and their temporal changes over time.

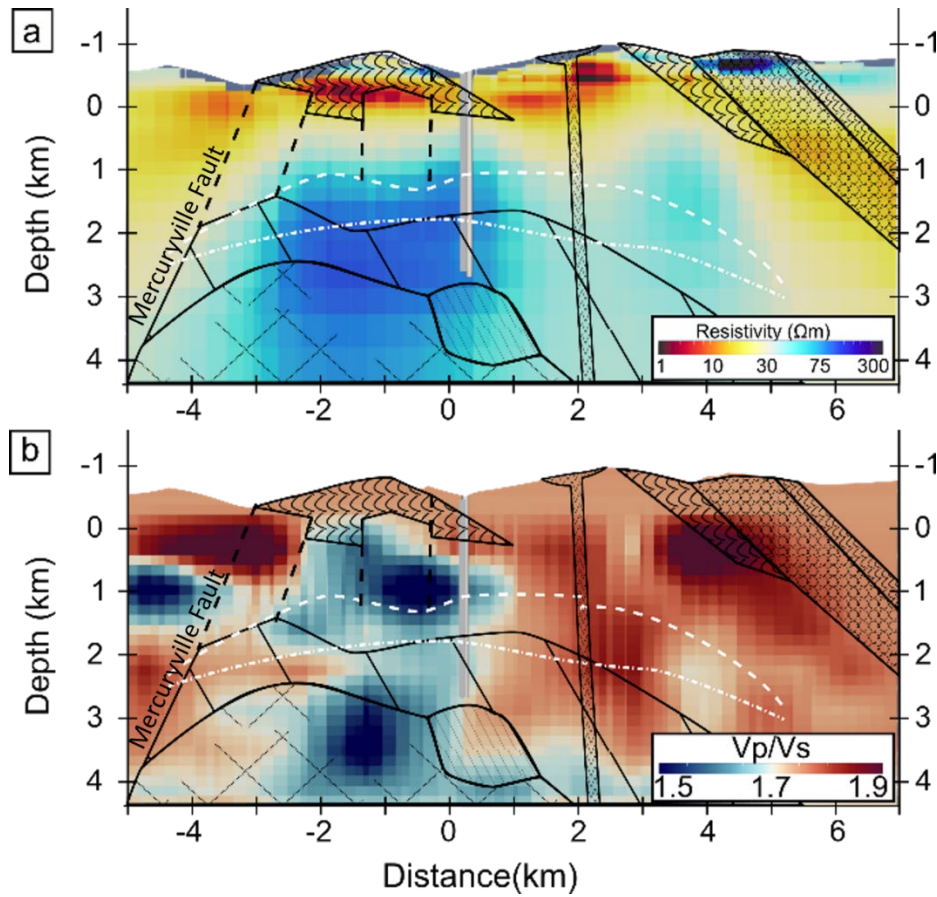
Therefore, the goal of the current project included the development of geophysical imaging techniques using seismic and magnetotelluric (MT) data to jointly image structural features and dynamic properties of the reservoir to support geothermal energy generation. The technical advancements of this project were provided via: (1) the monitoring of time-lapse changes in both seismic velocity and electrical conductivity that are occurring in the reservoir due to water injection and steam production; and (2) the joint inversion of the multi-physics (seismic and MT) data, which can provide images of the reservoir structure with higher confidence than can either of the data sets by themselves. Ultimately, these images can be used for better estimates of rock properties and spatial distribution of steam and water at

depth, for more accurate reservoir modeling and monitoring, and for more accurate placement of production wells.

The concept of the two complimentary geophysical techniques at The Geysers geothermal field is provided in Chapter 2, "Joint Inversion of Multiphysics Data." In a passive seismic tomography study at The Geysers geothermal reservoir, Gritto et al. (2013a) showed regions of low ratios of seismic P-wave to S-wave propagation velocities ( $V_p/V_s$ ) correlating with areas of high steam saturation, while high  $V_p/V_s$  ratios were found in regions that were subject to high rates of water injection to rehydrate the reservoir. The findings were supported through studies by Boitnott and Kirkpatrick (1997), Gritto and Jarpe (2014), and Gritto et al. (2023). Figure 1 displays this correlation. Figure 1a shows a southwest (SW) to northeast (NE) cross section of electrical resistivity (the inverse of conductivity) values across the reservoir (Peacock et al., 2020). In comparison, the  $V_p/V_s$  ratio along the same cross section is displayed in Figure 1b (Gritto et al., 2013a). The spatial correlation between low  $V_p/V_s$  and high electrical resistivity and, conversely, between high  $V_p/V_s$  and low electrical resistivity is rather apparent. The differences in the spatial extent of the anomalies between the two measurements along the margins of the survey areas are caused by the different spatial distribution of data receivers in the two geophysical surveys, as well as the differences in spatial sensitivity in the two different measurements. In addition, for the seismic  $V_p/V_s$  imaging, which is based on earthquakes as seismic energy sources, the associated earthquake locations were widespread throughout the reservoir, which enabled imaging the extension of the low  $V_p/V_s$  anomaly beyond the Mercuryville Fault at the SW end of the cross section (Figure 1b) despite the lack of seismic sensor in this area. This anomaly indicates the presence of steam outside the assumed reservoir boundaries, which was confirmed by steam production wells. Thus, low  $V_p/V_s$  and high electrical resistivity are spatially correlated to steam-saturated zones in the reservoir. In contrast, high  $V_p/V_s$  and low electrical resistivity are associated with water-saturated granitic intrusions, as indicated by the warm-colored regions in Figure 1. The example shows that the electrical and seismic measurements provide complementary insight into the subsurface for imaging steam and fluid saturation in geothermal reservoirs. Note that, in the current study, the team used electrical conductivity instead of electrical resistivity for its one-to-one correlation with  $V_p/V_s$ .

The combination of seismic and MT techniques to interrogate the state of the reservoir increases confidence in the interpretation of geophysical images that help operators to evaluate their reservoir management and to better understand their use of the geothermal resource, including water injection, steam production, and well-planning operations.

**Figure 1: Cross Sections Through The Geysers Geothermal Reservoir from SW to NE**



**Cross sections through The Geysers geothermal reservoir from the SW to the NE, showing a) electrical resistivity and b) the  $V_p/V_s$  ratio. Black lines denote geological formations in the reservoir. The long-dashed white line denotes the top of steam and the short-dashed white line denotes the top of the hot dry rock reservoir. See the text for further explanation.**

Source: Peacock et al., 2020

## **CHAPTER 2:**

# **Project Approach**

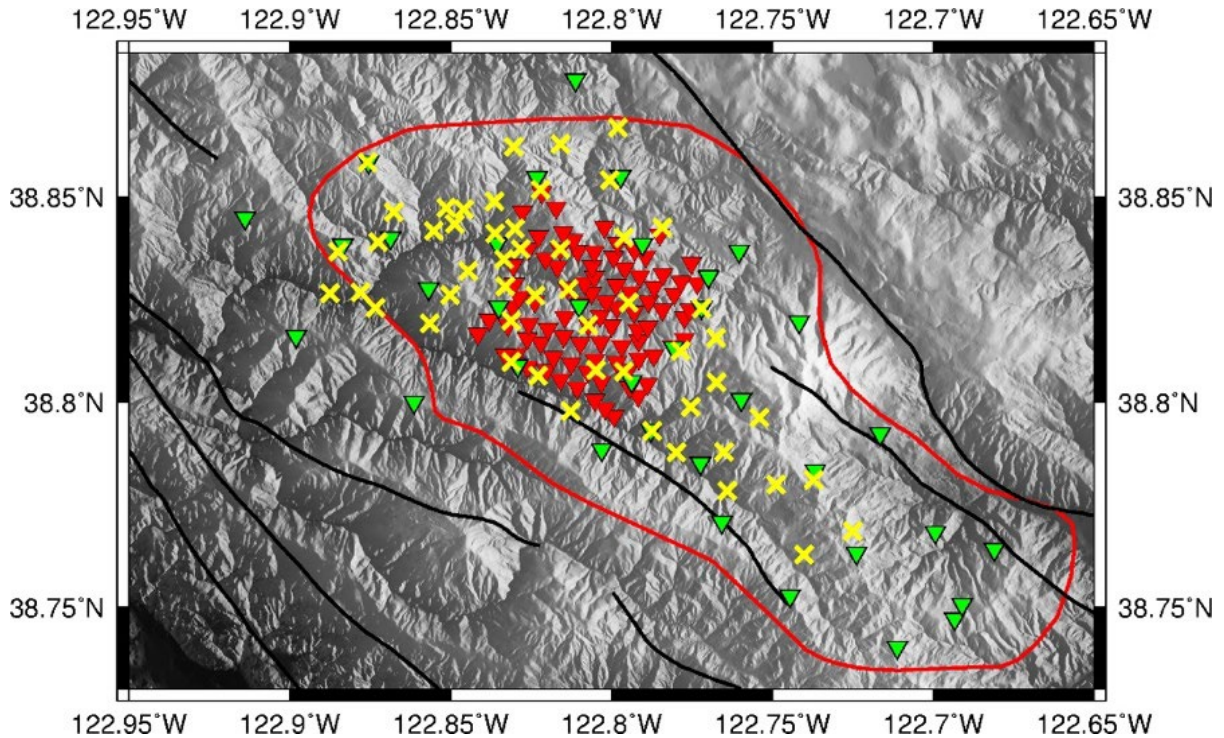
---

The current project was a collaboration between the Lawrence Berkeley National Laboratory, the United States Geological Survey, EMR Solutions and Technology (formerly Array Information Technology) and Jarpe Data Solutions. The Lawrence Berkeley National Laboratory team was comprised of Dr. David Alumbaugh (PI, electric/MT imaging), Dr. Evan Um (joint inversion of seismic and MT data), and Craig Ulrich (correlation of geophysical images with reservoir structure), while Dr. Jared Peacock (electrical/MT methods) led the United States Geological Survey component. Dr. Roland Gritto (co-PI, seismic imaging) of EMR Solutions and Technology and Steve Jarpe (seismic data processing) of Jarpe Data Solutions completed the research team. The team was advised by the Technical Advisory Committee members Professor Douglas Dreger (University of California, Berkeley, seismic analysis), Dr. Randall Mackie (CGG, electric/MT imaging) and Craig Hartline (Calpine Corporation, interpretation/use of seismic data for construction of 3D geothermal reservoir model).

The objectives of this project were to use a combination of MT and seismic data to characterize the 3D structure of the geothermal reservoir at The Geysers, with an emphasis on delineating water and steam concentrations to support the operators managing their use of the resource including water injection, steam production, and well-planning operations. The tasks of this three-year project were to: (1) continuously record micro-earthquake data over The Geysers geothermal field using two installed seismic data acquisition networks, as shown in Figure 2; (2) acquire three time-lapse MT surveys at one-year intervals in the same area using a surface array of MT receivers (Figure 2); (3) jointly invert these time-lapse data for images of seismic velocities and electrical conductivity at the three different times, using workflows and algorithms that enforce structural similarity constraints between the different physical properties; and (4) correlate the single and joint-inversion geophysical images to the Geysers 3D reservoir model. The technical advancements of this project are provided via: (1) the monitoring of time-lapse changes in both seismic velocity and conductivity that are occurring in the reservoir due to water injection and steam production; and (2) the joint inversion of the multi-physics data, which can provide images of the reservoir structure with increased confidence compared to either of the data sets by themselves. Ultimately, these images can be used for better estimates of rock properties and spatial distribution of steam and water at depth, for more accurate reservoir modeling and monitoring, as well as for more accurate placement of production wells.



**Figure 2: Map of The Geysers With Locations of Seismic and MT Stations**



**Map showing an outline of The Geysers steam field (red polygon), the locations of the two seismic networks currently in operation at The Geysers geothermal reservoir, and the MT sites. The yellow crosses represent 52 MT locations, while the 35 green triangles and the 91 red triangles denote the locations of the seismic stations belonging to the permanent network and the temporarily deployed CEC dense seismic network, respectively. Note that some of the sites of the permanent network housed surface and borehole stations, such that the total number of permanent seismic stations amounts to 49. The black line represents surface traces of known faults in the region.**

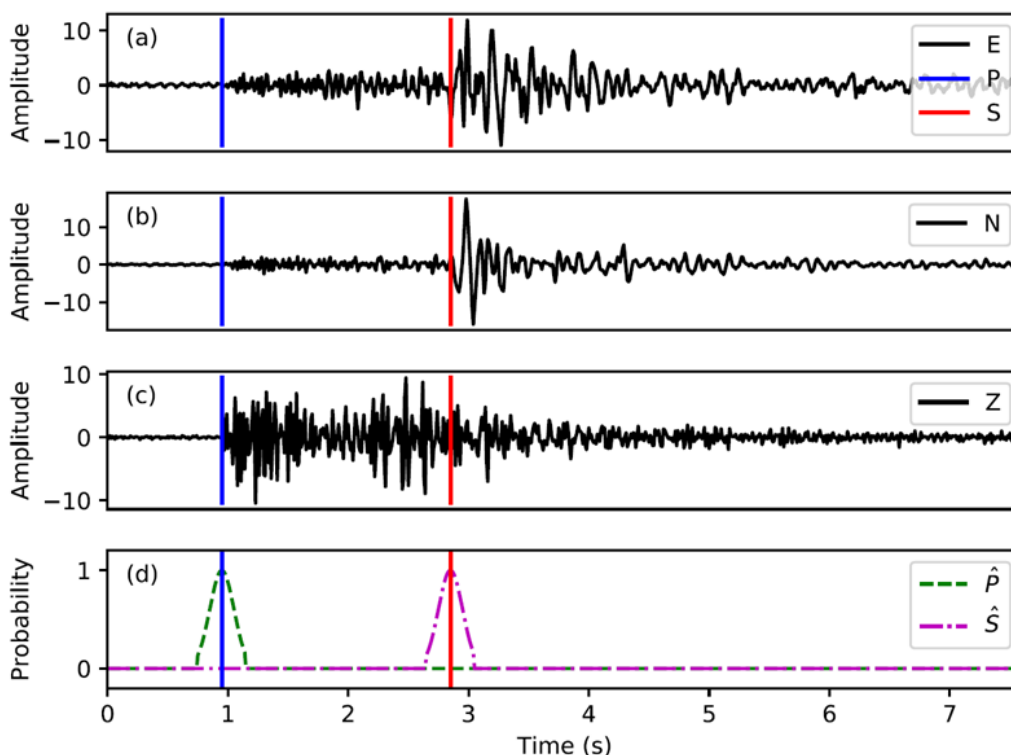
Source: Gritto et al., 2024

## **Passive Seismic Data Acquisition and Processing**

The goals of this task included collecting, processing, and tomographically imaging passive seismic earthquake data at The Geysers geothermal reservoir to generate a baseline of seismic attributes and to investigate possible spatio-temporal variations within the reservoir. The outcome of this task served as input for the joint seismic and MT imaging of this project and for the reservoir correlation analysis.

During this task, the team collected, processed, and tomographically imaged passive seismic earthquake data, the temporary CEC-seismic network, and the permanent BG-seismic network that are currently operating at The Geysers geothermal reservoir. (For details on the temporary CEC-seismic network, see Appendix C.) The seismic data were automatically processed with an analysis package based on artificial intelligence. The processing routine included PhaseNet (Zhu and Beroza, 2019), a deep-neural-network-based seismic arrival-time picking method, and the Gaussian Mixture Model Association (GaMMA), an event association and preliminary location module. PhaseNet uses three-component seismic waveform data as input and generates probability distributions of P-wave and S-wave arrivals as output. The maxima in the probability distributions provide accurate arrival times for both seismic P-waves and S-waves, as shown in Figure 3.

**Figure 3: Seismic Traces With Detections of Seismic Phase Arrival by PhaseNet**



**Trace sample with PhaseNet phase detections. Seismograms (a) through (c) show east, north, and vertical components, respectively. The blue and red vertical lines are the manually picked P- and S-arrival times. (d) shows the result of PhaseNet in the form of converted probability masks for P- and S-picks output.**

Source: Gritto et al., 2024

The phase data and preliminary earthquake locations were subsequently used to perform 3D joint inversion for P-wave and S-wave velocity structure and hypocenter locations using the inversion code *tomofDD* (Zhang and Thurber, 2003; Gritto et al., 2023). The code performs joint inversion of the velocity structure, as well as absolute and relative earthquake hypocenter locations, using absolute and differential (double-difference) travel times. The results are combined to form 3D images of the  $V_p/V_s$  heterogeneity in the reservoir and accurate hypocenter locations, which can be used to interpret the structure and the distribution of water or steam in the reservoir.

The seismic data collection and processing resulted in the highest number of events detected and processed over a five-year period at The Geysers geothermal reservoir to date. This was based on data collected from June 2018 to April 2023 under a previous CEC-sponsored project (EPC-16-021, Gritto and Nakagawa, 2020) and under the current project. The processing of the recorded seismic waveforms resulted in the location of 224,000 earthquakes with 8,300,000 P-wave and 8,700,000 S-wave arrival times. By combining the two seismic networks and because of the unprecedented data density, the team obtained the highest resolution and the best spatial coverage on a reservoir-wide scale to date, which improved the seismic imaging results at The Geysers geothermal field.

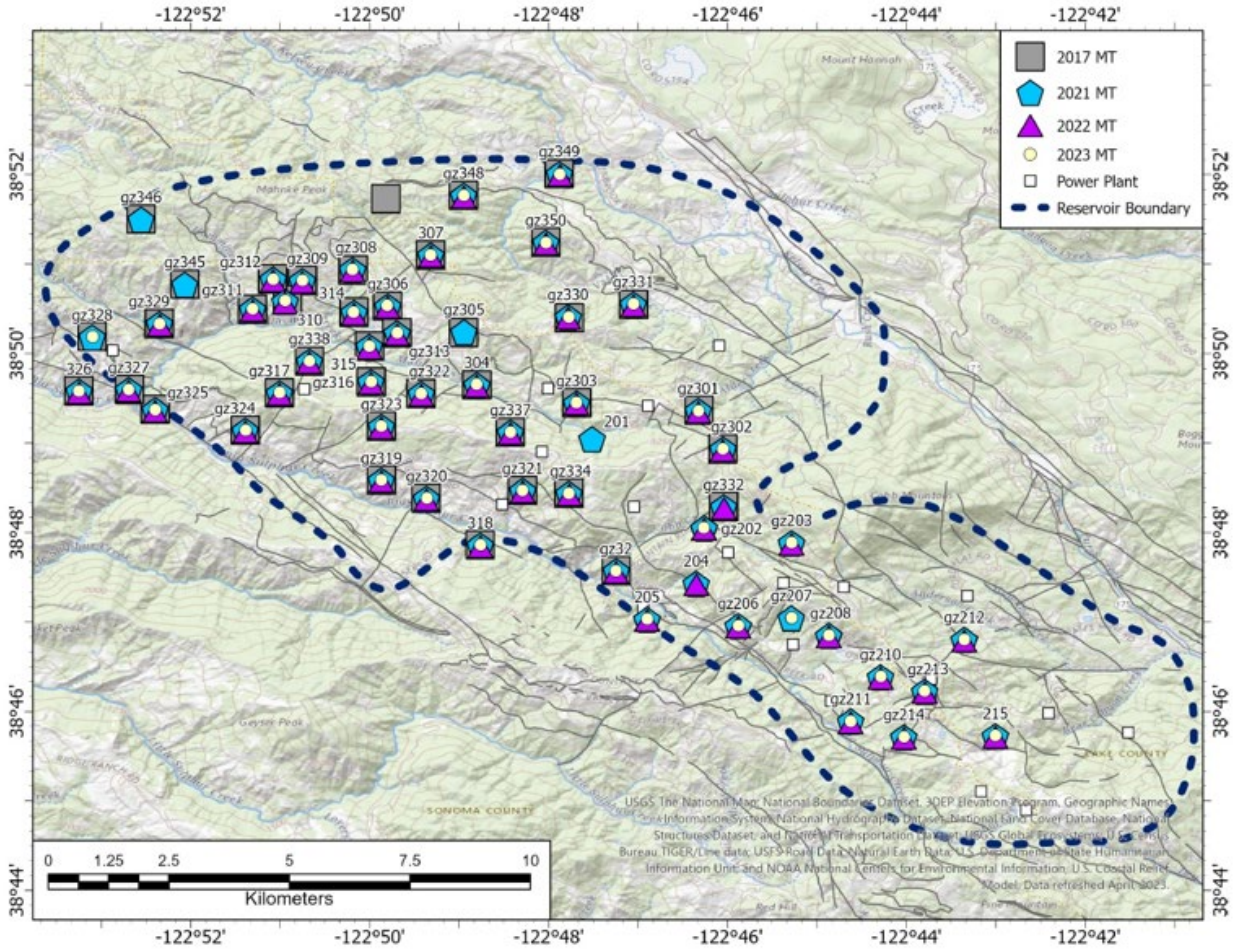
## **Magnetotelluric Data Acquisition and Processing**

The aim of this effort was to collect MT data at The Geysers geothermal field during three periods in April 2021, April 2022, and April-May 2023 and to process these data for MT imaging of reservoir properties. Data from 50 to 55 repeating station locations were collected during each field campaign to enable absolute and time-lapse imaging of properties and processes in the reservoir. Figure 4 shows a map of The Geysers, with the outline of the steam field given by the blue dashed line, the locations of the MT sites during the annual campaigns given by the gray squares, blue pentagons, and magenta triangles, and the locations of the power plants indicated by the small yellow squares. For most stations, repeat measurements were obtained during each survey. The results were also compared to an MT survey that took place in 2017 (gray squares in Figure 4), which provided the option to investigate temporal changes over a longer time period.

MT is a passive electromagnetic method that measures the earth's electrical response to natural time-varying magnetic fields (Chave and Jones, 2012). The ratio of measured electric and magnetic fields is inherently related to subsurface electrical resistivity through the MT transfer function, which is directly sensitive to fluids. This makes MT a powerful complimentary technique with measurements sensitive to the rock matrix like gravity and seismic methods (Peacock et al., 2020).

Each MT station included two horizontal orthogonal magnetic induction coils and two orthogonal electrical dipoles with a nominal length of 50 meters, dependent on vegetation and topography (Figure 5). Electric potentials were measured with electrodes placed in a saturated canvas bag of bentonite clay to reduce contact resistance with the soil. The entire setup was oriented with geomagnetic north. The four components were connected to a 5-channel 32-bit data logger, and data were recorded on a repeating schedule of 5 hours and 50 minutes. The schedules were set such that all recording instruments recorded synchronously to allow for remote reference processing.

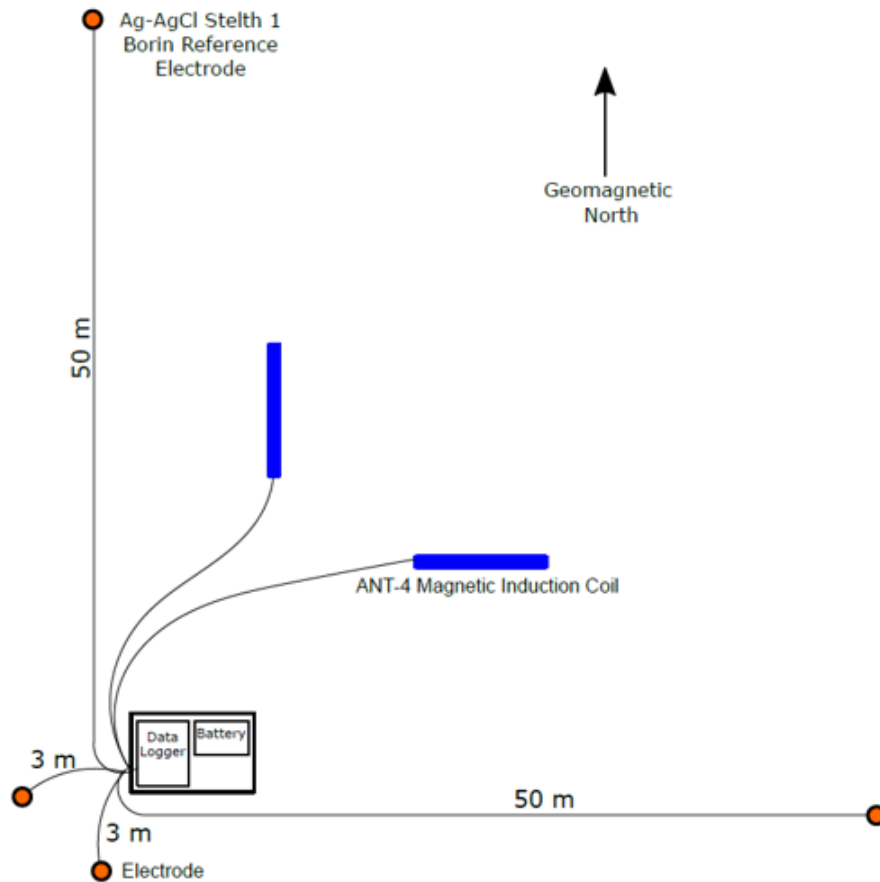
**Figure 4: Map With MT Sites of the Annual Surveys**



**Map showing the outline of the steam field (dashed blue line), with the MT sites of the annual surveys and power plants at The Geysers geothermal reservoir.**

Source: Gritto et al., 2024

**Figure 5: Geometry of an MT Station**



**Geometry with the layout of a typical MT station during the MT surveys at The Geysers geothermal field.**

Source: Gritto et al., 2024

The MT data were first analyzed in the time domain, looking at the time series data, spectra, and spectrograms, to identify bad data. Quality data can be characterized as having a relatively smooth frequency spectrum. Naturally, the power spectrum increases for lower frequencies, while a dead band occurs between 0.1-1 Hz, where there is naturally a low signal.

The MT data can be analyzed by way of the MT transfer function, which is a matrix as a function of frequency, where lower frequencies are sensitive to deeper structures as MT is a diffusive method. To estimate the MT transfer function, the time series data were first transformed into the frequency domain, where incoherent noise is removed by comparison to remote reference stations, at which data are assumed to be stationary over time. In a noisy environment like The Geysers, this is of great importance. The temporal changes of the MT transfer function, referred to as the MT residual phase tensor, are shown in Chapter 3, "Magnetotelluric Data Acquisition and Processing."

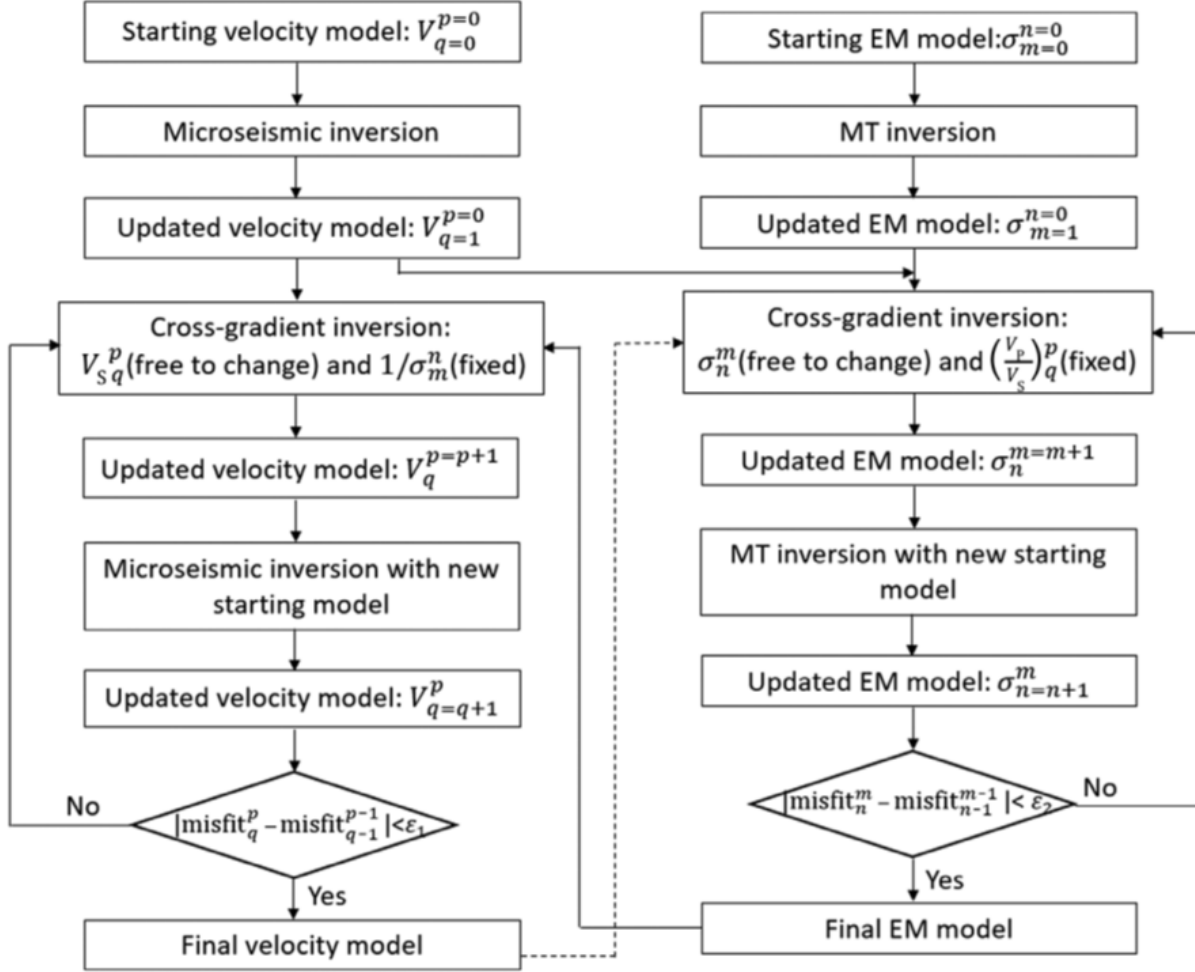
## **Joint Inversion of Multiphysics Data**

During this task, the team performed a joint inversion of the seismic and MT data that were concurrently acquired at The Geysers geothermal field. The goal was to enhance the reliability

of the imaging results and the consistency between the two geophysical images, which enabled the team to examine spatio-temporal changes in the geothermal reservoir with increased precision and confidence. The team inverted the seismic and MT data collectively using a 3D cooperative joint inversion method (Um et al., 2014, 2023). In this project, the team applied the workflow using seismic and MT data to examine if the joint inversion could improve the overall resolution and reliability of the geophysical models to accurately characterize the distribution of water and steam in the geothermal system.

The joint inversion aims to find a set of more consistent earth property models (e.g., seismic wave velocity and electrical conductivity) by simultaneously fitting multiple sets of geophysical data to the models. Commonly used joint inversions can be grouped into two approaches. One approach uses petrophysical relationships to link multiple geophysical attributes (e.g., Harris and MacGregor, 2006; Hoversten et al., 2006). The other approach is based on the structural similarity among different geophysical property models (Haber and Oldenburg, 1997; Gallardo and Meju, 2003; Gallardo and Meju, 2007), which the team used in the current project. The joint inversion approach, based on structural similarities, is well-suited to imaging geothermal fluids and steam at The Geysers, because seismic velocity and electrical conductivity models are expected to have structural similarities. Accordingly, using a similarity constraint, the joint inversion can find a set of velocity and conductivity models that are consistent with each other (Um et al., 2023). The schematics of the joint inversion are provided in Figure 6, which shows a flow chart of the joint inversion workflow (Um et al., 2014). The workflow shows how the misfit between the observed and modeled seismic and MT data is minimized and the respective results are inserted into the cross-gradient inversion of the opposite workflow.

**Figure 6: The Joint Inversion Workflow**



**The joint inversion workflow (Um et al., 2023). Here,  $V$  and  $\sigma$  are seismic and conductivity models, respectively. Their superscript and subscript represent the number of joint inversions and standalone inversions performed during the inversion process.**

Source: Gritto et al., 2024

Seismic and MT inversion resolution can vary, depending on sensor spacing and distribution and on data quantity and quality. High-frequency MT data can have high resolution in the shallow subsurface. However, from 1 kilometer (km) to 5 km depth at The Geysers, where the number of earthquakes is highest, the inversion of seismic data based on high spatial sensor coverage produces images of the geothermal reservoir with higher resolution than MT inversion (Gritto et al., 2023; Peacock et al., 2020). Accordingly, it is reasonable to first infuse structural information from the seismic inversion model to the MT inversion model. This is realized by fixing the velocity model (i.e.,  $V_p/V_s$ ) as a reference model, while the conductivity model is free to change. The resulting conductivity model resembles the  $V_p/V_s$  model but likely shows a large data misfit because the inversion does not include the data portion. To reduce the data misfit, the resulting conductivity model is used as a new starting model for a subsequent standalone MT inversion, with the goal of preconditioning an MT starting model with structural information from the seismic inversion model. The refinement process and the subsequent MT inversion are stopped when the MT data misfit no longer decreases. The joint

inversion was applied to seismic and MT data concurrently collected in 2021, 2022, and 2023. The results are shown in Chapter 3, “Joint Inversion of Multiphysics Data.”

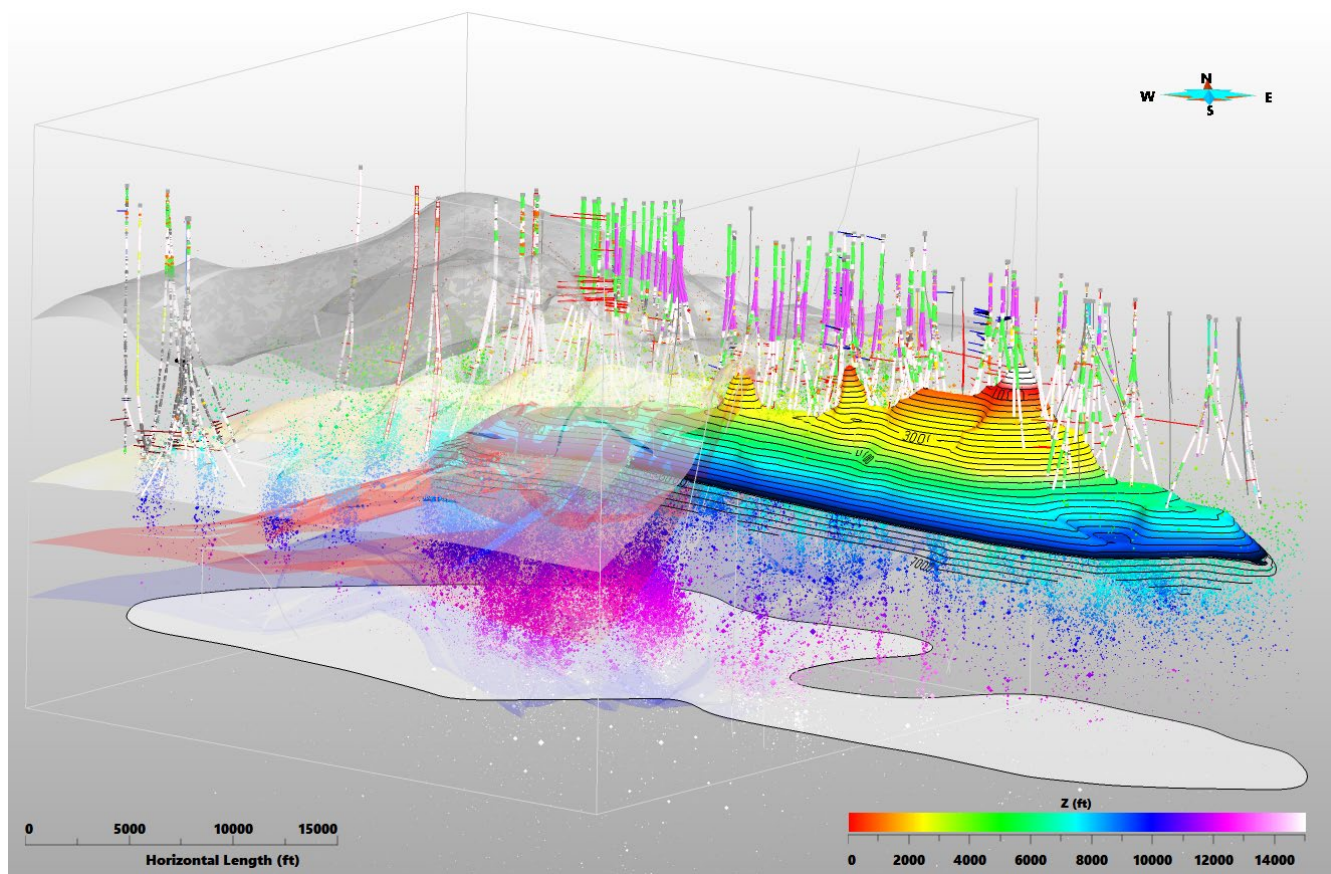
## **Appraising Geophysical Data Through Geothermal Reservoir Model**

The temporal and spatial information provided by seismic and MT measurements can be used to improve the understanding of the physical processes in a geothermal reservoir by measuring the effects of water and steam saturation on seismic wave velocities and electrical conductivity. The physical effects include high  $V_p/V_s$  and electrical conductivity for water-saturated areas and low  $V_p/V_s$  and electrical conductivity for steam-dominated areas. As such, these two physical measurements are complementary in that they measure different physical properties to estimate the same reservoir parameters. Knowledge of the spatial distribution and temporal variation of water and steam concentrations can inform decisions on reservoir planning and operations.

The appraisal of the geophysical images obtained through single and joint inversion of seismic and MT data is done by spatial correlation with the 3D reservoir model of The Geysers geothermal field. The reservoir model was developed using in situ information from hundreds of boreholes throughout The Geysers and from the distribution of earthquakes associated with water injection into the geothermal reservoir. Calpine Corporation’s (Calpine) 3D pre-drilling analyses and detailed 3D fracture zone interpretations indicated the potential to utilize induced seismic events, including those seen on synchronized water injection, as a significant constraint on The Geysers’ 3D structural model development. Induced seismicity patterns and seismic event density variations appear to be indicative of permeability variations and resulting fluid flow, allowing the interpretation of fracture zones and lithological changes. For example, the transition from hornfelsic graywacke to felsite, which represent the two main geological rock types in The Geysers, generally correlates with a decrease in seismic event density in the west-central and southeast Geysers (Hartline et al., 2015, 2016). The fact that the top felsite markers, based on drilling information, and the seismic event density transition are spatially consistent increases Calpine’s confidence in the utilization of seismic event hypocenters as an additional constraint on top felsite surface development and 3D structural model development in general (Hartline et al., 2015, 2016). During the appraisal of the geophysical imaging results, the team incorporated estimates of the  $V_p/V_s$  ratio and electrical conductivity into the 3D reservoir model to allow for spatial correlation analyses. The complex 3D reservoir model consisted of four major sub-horizontal interfaces, including top of steam, top of hornfelsic graywacke, top of felsite and base of steam. These interfaces are intersected by a network of sub-vertical faults that strike northwest and northeast. In addition to the geological information, the model contained water injection and steam production data obtained from observations from hundreds of boreholes throughout the reservoir. Figure 7 shows details of the 3D reservoir model, including major geological interfaces, trajectory of boreholes, and seismicity hypocenter locations.



**Figure 7: The Geysers 3D Structural Reservoir Model**



The Geysers 3D structural model as viewed from the south. Displayed are the following surfaces separating the major geologic layers from top to bottom: top of graywacke (gray), top of hornfelsic graywacke (tan), top of granitic felsite intrusion in the northwest (red), and base of the reservoir (blue). Also shown are: the borehole trajectories, with the color denoting the major geologic layers (green: greenstone; magenta: serpentinite; and light pink: graywacke); the top interface of the felsite granitic intrusion in the southeast Geysers (rainbow-colored by depth from 0 to 6,000 feet); and the earthquake hypocenter locations, color-coded by depth. The white shading at the bottom denotes the outline of the steam reservoir projected to a 20,000-foot depth. The color scale at the bottom represents the depth of seismicity. The vertical exaggeration is 1.25.

Source: Gritto et al., 2024

# CHAPTER 3:

## Results

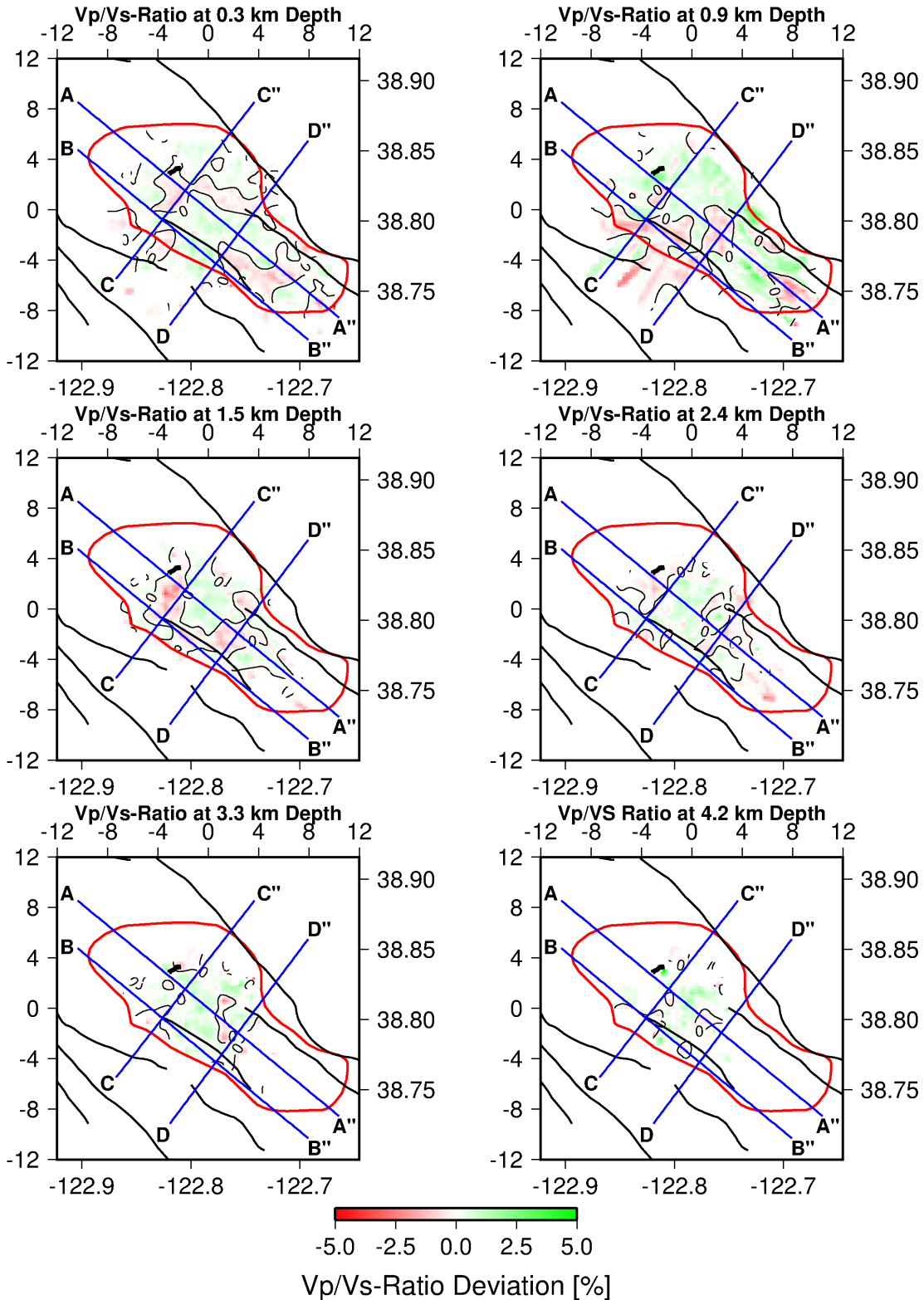
---

### Passive Seismic Data Acquisition and Processing

In the following section, results from 3D seismic imaging of the temporal changes in the  $V_p/V_s$  ratio are presented by comparing data collected from May 2018 to December 2019 with data collected in 2020. However, when conducting time-lapse seismic imaging, careful attention needs to be given to the data processing before imaging results from two epochs can be compared. The time-lapse results shown below are based on the approach by Gritto et al. (2013b), which is described in Appendix A. The resulting time-lapse images of the  $V_p/V_s$  ratio are shown in Figure 8 and Figure 9. Figure 8 displays horizontal cross sections of differential  $V_p/V_s$  ratios in percent throughout The Geysers reservoir. This means positive changes (green colors) refer to temporal increases in  $V_p/V_s$  and thus potential increases in water saturation, while negative changes (red colors) refer to temporal decreases in  $V_p/V_s$  and potential increases in steam concentration. The most pronounced changes are observed in the upper 2.4 km, where the effects of reservoir operations from water injection and steam production wells are most noticeable. The blue lines denote profiles along which vertical cross sections through the reservoir are calculated. The results along these profiles are shown in Figure 9. The strongest temporal changes are visible in profiles A-A'' and B-B'' in the upper section of the reservoir in the hornfelsic graywacke formation above the felsite intrusion in the reservoir. The temporal changes are less than 5 percent, which is reasonable considering the short time-span between the measurements. Gritto et al. (2013b) studied the temporal changes in  $V_p/V_s$  throughout The Geysers between 2005 and 2011, with the intention of estimating the effects of resupplying the reservoir with water after the inception of the South-East Geysers Effluent Project pipeline project in 2004. They found maximum increases of 3 percent to 5 percent in  $V_p/V_s$  in the vicinity of water injection wells.

Results for the time-lapse imaging between 2023 and 2018.2019 are provided in Appendix A.

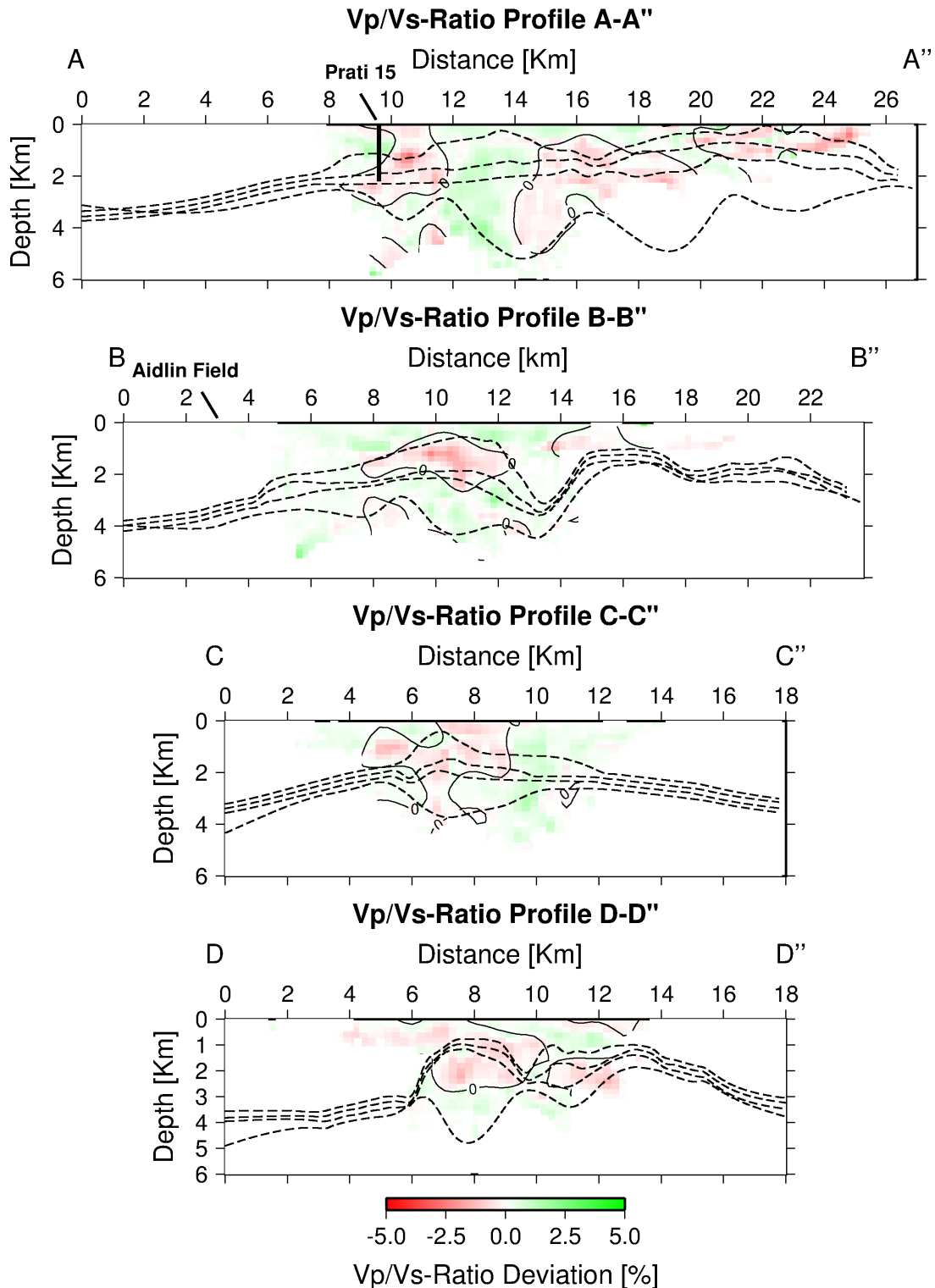
**Figure 8: Horizontal Slices of Temporal Changes in Vp/Vs**



Horizontal slices of the temporal changes in Vp/Vs when differentiating the 2020 and 2018.2019 results (2020-2018.2019). The results are shown only for regions that have sufficient ray coverage, as determined by the derivative weight sum (DWS). The outline of the steam reservoir is given by the red polygon, while the black lines represent surface traces of known faults in the region.

Source: Gritto et al., 2024

**Figure 9: Vertical Cross Sections of Temporal Changes in Vp/Vs**



Vertical slices through the profiles are indicated by the blue lines in Figure 8. The results represent the temporal changes in Vp/Vs when differentiating the 2020 and 2018.2019 results (2020-2018.2019) and are shown only for regions that have sufficient ray coverage, as determined by the DWS. The dashed lines denote, from top to bottom, the top of the steam reservoir, the top of the hornfelsic graywacke, the top of the felsite intrusion, and the base of the steam reservoir.

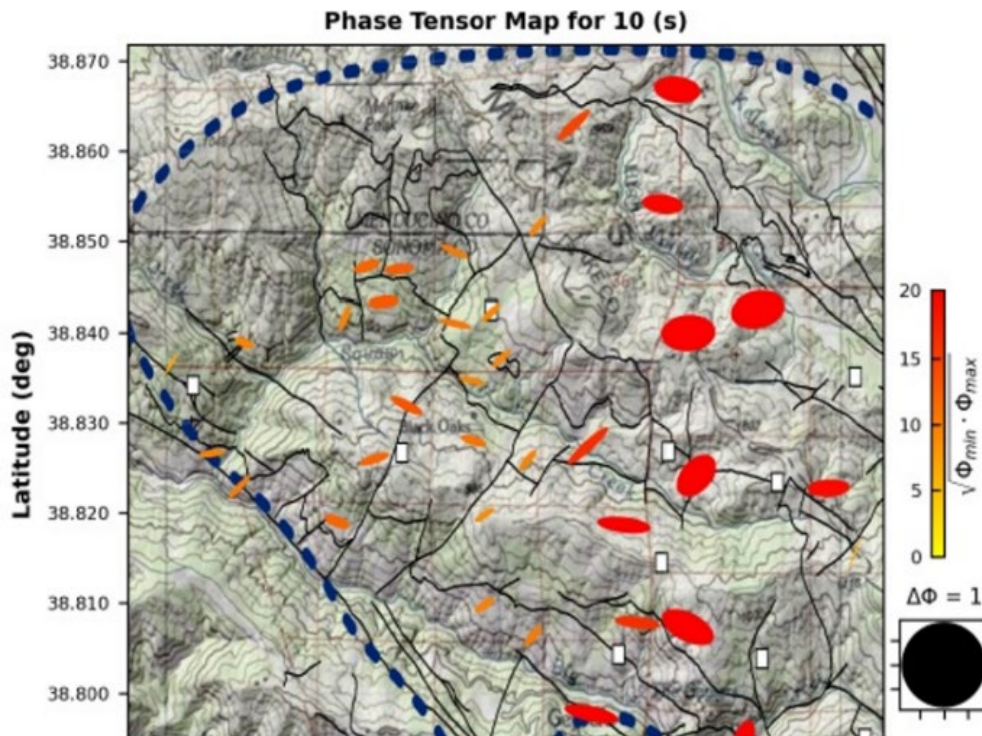
Source: Gritto et al., 2024

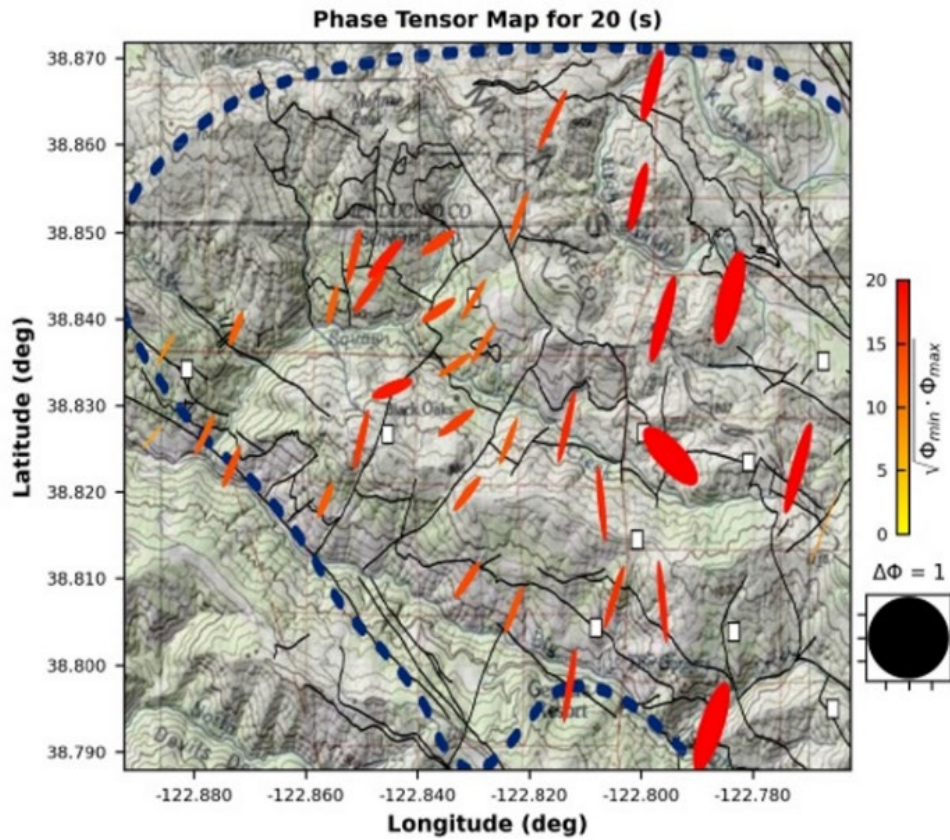
## Magnetotelluric Data Acquisition and Processing

The phase tensor that was mentioned in Chapter 2, "Magnetotelluric Data Acquisition and Processing," provides a distortion-free representation of the MT transfer function (Caldwell et al., 2004). In the current project, a residual phase tensor was estimated between repeat surveys (Peacock et al., 2012). The graphical representation is an ellipse, where the shape describes how the subsurface or new infrastructure changed between the two surveys. A circle indicates a uniform change in all directions, while an elongated ellipse indicates a change in the direction of the larger axis. The color represents an average percent change. Data periods from 2 seconds to 50 seconds are approximately the range where changes in the reservoir would occur. The residual phase tensors in Figure 10 and Figure 11 show estimates for each of the 37 stations in the northwest Geysers that were repeated between 2017 and 2023.

Figure 10 displays the residual phase tensor for 10 seconds and 20 seconds. Around 10 seconds, the western part of the survey area aligns with a northwestern direction, whereas the eastern side of the survey aligns more north-south, suggesting compartmentalized changes in the shallow part of the reservoir over five years. As the period becomes longer (Figure 11), the residual phase tensors become more aligned in a northeastern direction. The results of the phase tensor are superimposed on topographic maps, with known fault locations indicated by the black lines. Inspecting these faults reveals that the longer axes of the residual phase tensors align with the strike directions of the faults in the majority of cases. The spatial correlation of the residual phase tensor parallel to the strike of the faults may indicate that temporal changes, such as those generated by water injection, may have occurred along these faults. That is, the faults may have served as barriers to lateral water migration.

**Figure 10: Residual Phase Tensor Maps for Periods of 10 Seconds and 20 Seconds**

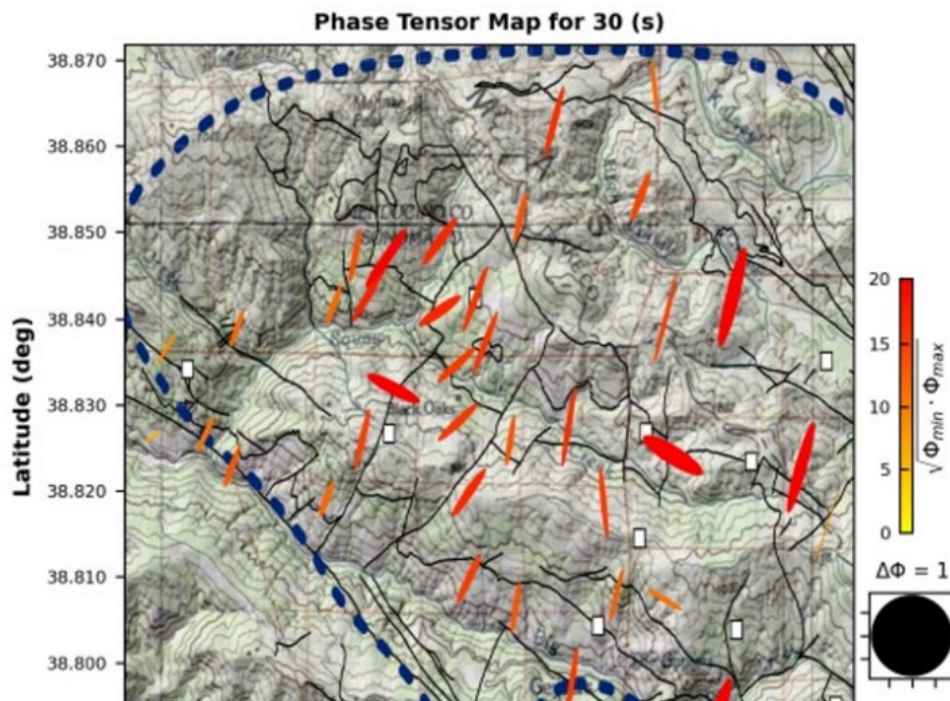


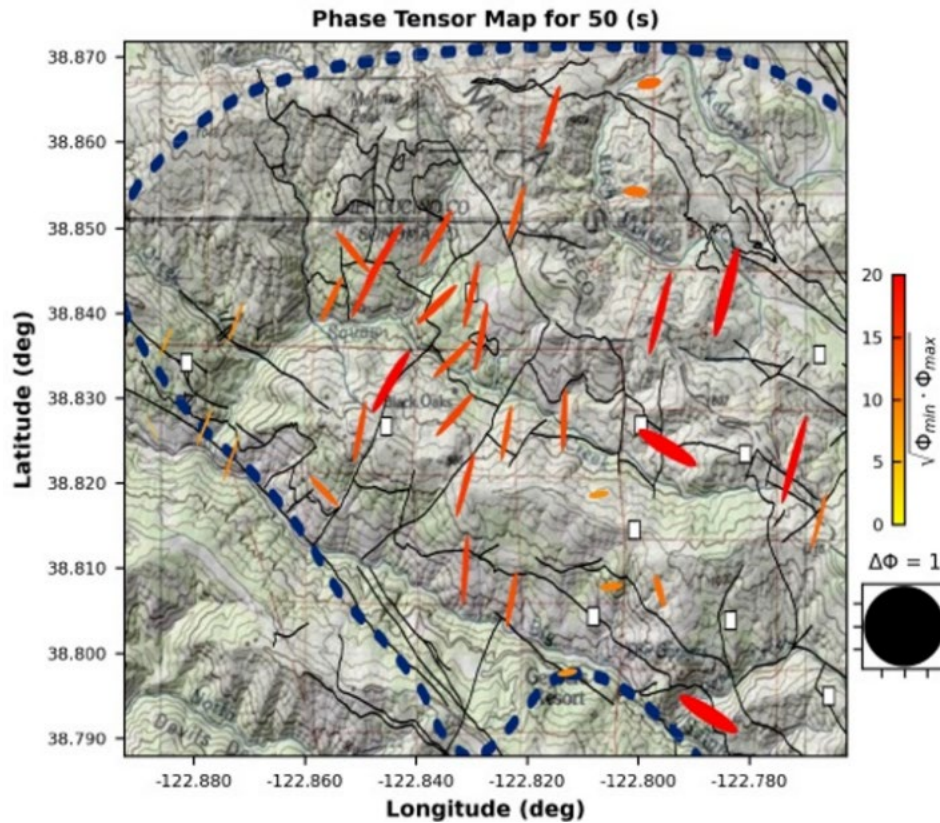


**Residual phase tensors for periods of 10 seconds and 20 seconds, plotted on topographic maps in The Geysers geothermal field. The phase tensors show the difference between the MT data recorded in 2017 and 2023 and may indicate temporal changes in the geothermal reservoir.**

Source: Gritto et al., 2024

**Figure 11: Residual Phase Tensor Maps for Periods of 30 Seconds and 50 Seconds**



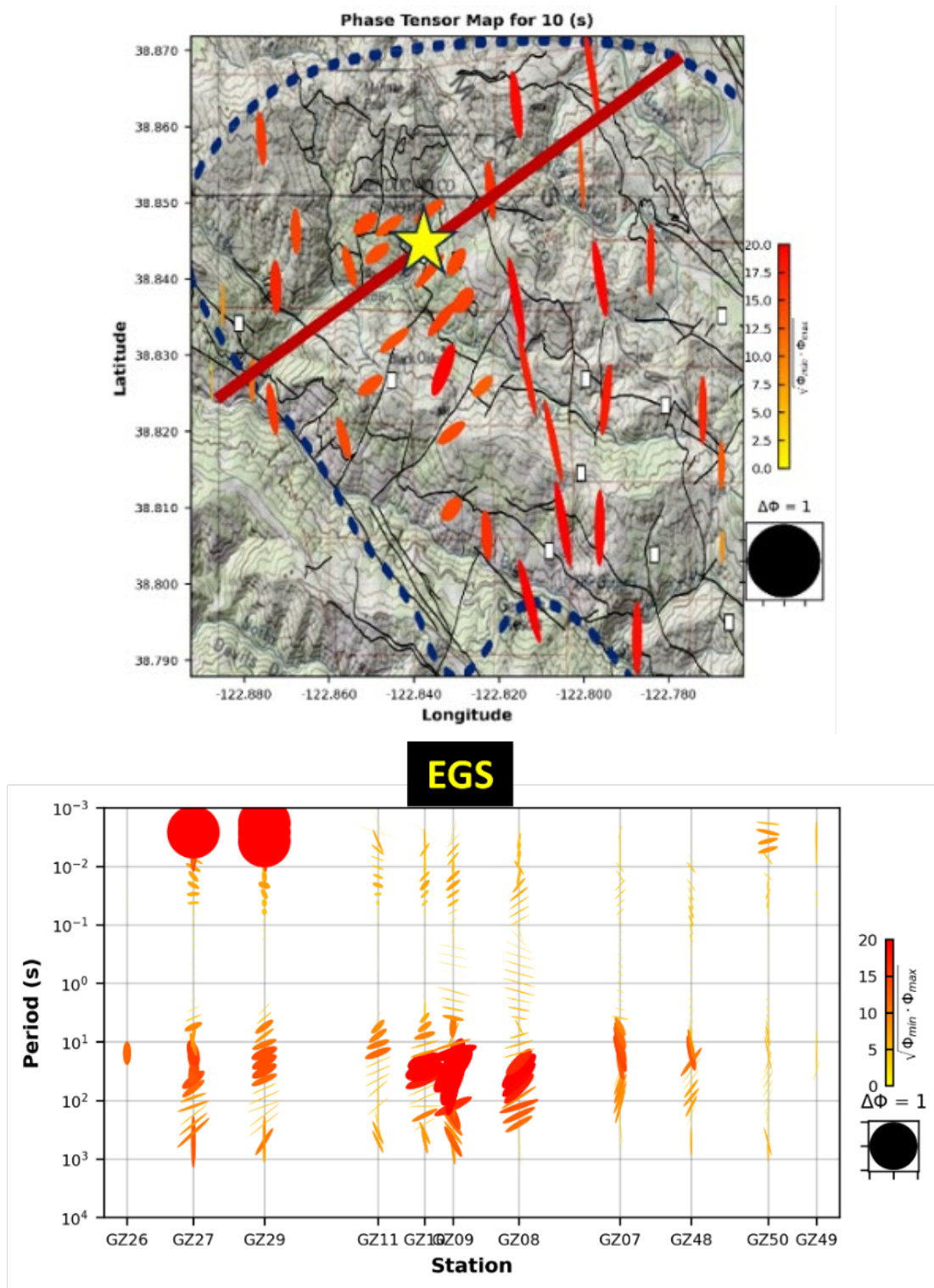


**Residual phase tensors for periods of 30 seconds and 50 seconds, plotted on topographic maps in The Geysers geothermal field.**

Source: Gritto et al., 2024

A closer look at the residual phase tensors between the 2017 and the 2021 MT surveys is shown on the left-side map in Figure 12, where the yellow star denotes the location of the enhanced geothermal system (EGS) in the northwest Geysers (Hartline et al., 2019b). The red line denotes a transect across the EGS system and along several stations in the northwest Geysers. The residual phase tensors along this cross section are plotted in the right diagram in Figure 12, which shows the station location at the bottom and the period on the abscissa. The location of the EGS system is indicated at the top of the diagram. The largest changes at depth are associated with stations GZ08, GZ09, and GZ10, which were located in the vicinity of the EGS system. The associated periods range between 10 seconds and 100 seconds, which matches the depth of the EGS system.

**Figure 12: Residual Phase Tensor for Period of 10 Seconds on Map and in Cross-Sectional View**



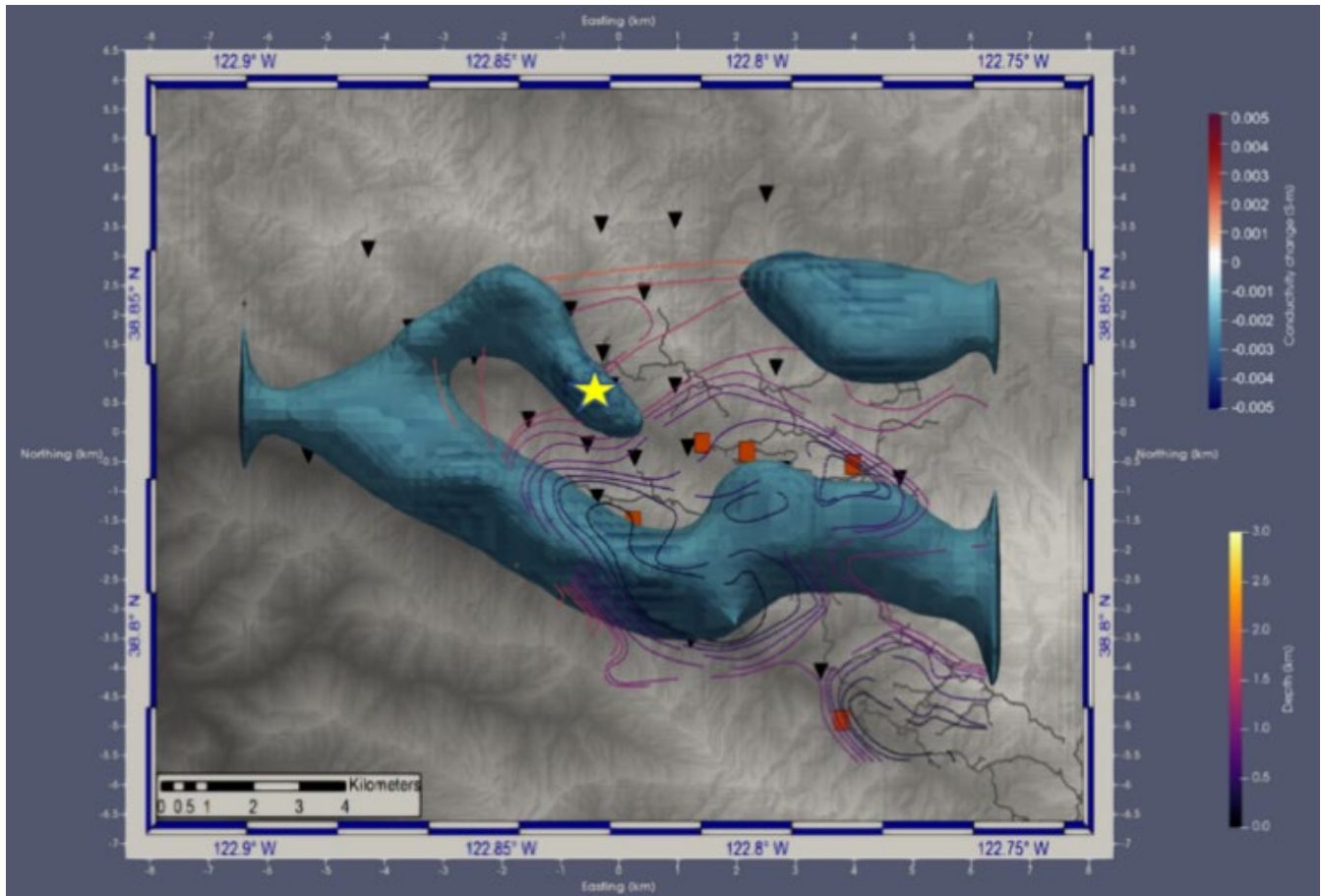
**Left: A residual phase tensor for a period of 10 seconds, plotted on a topographic map of The Geysers geothermal field. The yellow star denotes the location of the Prati 32 EGS project. Right: A residual phase tensor plotted along the transect, shown by the red line on the map. The location of the EGS site is denoted on top.**

Source: Gritto et al., 2024



The previous findings are supported by the results in Figure 13, which shows an iso-surface plot of the temporal change in electric resistivity between the 2017 and the 2021 MT surveys. The iso-surface represents a negative resistivity change of approximately  $-35 \Omega\text{m}$ , which can be explained by an increase in water volume at depth, due to continued water injection from 2017 to 2021. The location of the EGS system is indicated by the yellow star and correlates with a pronounced resistivity decrease. It is therefore likely that the observed changes in Figure 12 and Figure 13 are due to the continuous injection of water in the area.

**Figure 13: Iso-Surface Plot With Change in Electrical Conductivity Between 2017 and 2021**



**Iso-surface plot representing a negative conductivity change of approximately  $-0.003$  Siemens per meter (S-m) between 2017 and 2021.**

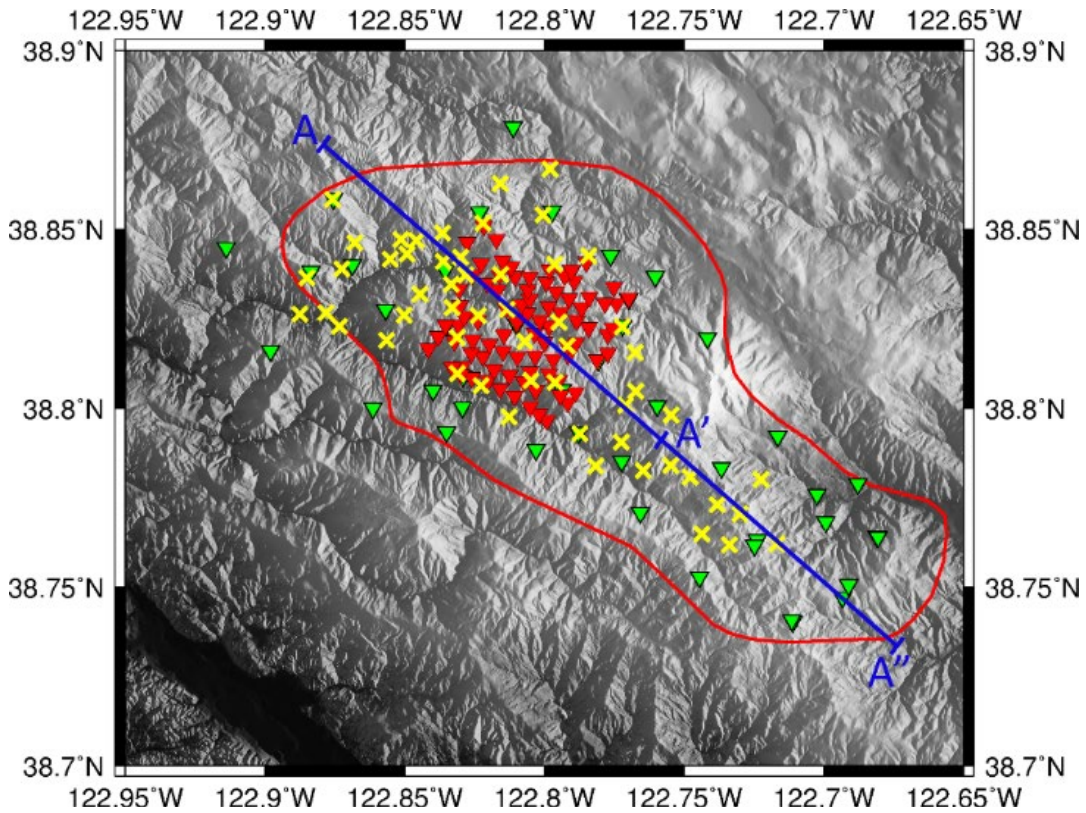
Source: Gritto et al., 2024

## Joint Inversion of Multiphysics Data

At The Geysers, the project team anticipated structural similarities between seismic velocity and electrical conductivity models, with high  $V_p/V_s$  correlating to high conductivity and low  $V_p/V_s$  correlating to low conductivity. Based on these observations, our joint inversion exploited a cross-gradient constraint (Gallardo and Meju, 2003) to identify velocity and conductivity models that align structurally, thereby improving consistency between velocity and conductivity models and further reducing data misfit.

In the following section, the results of the joint inversion of seismic and MT data are discussed for the cross section along the short profile A-A' in Figure 14.

**Figure 14: Map With the Location of Seismic and MT Stations and Two Profiles**



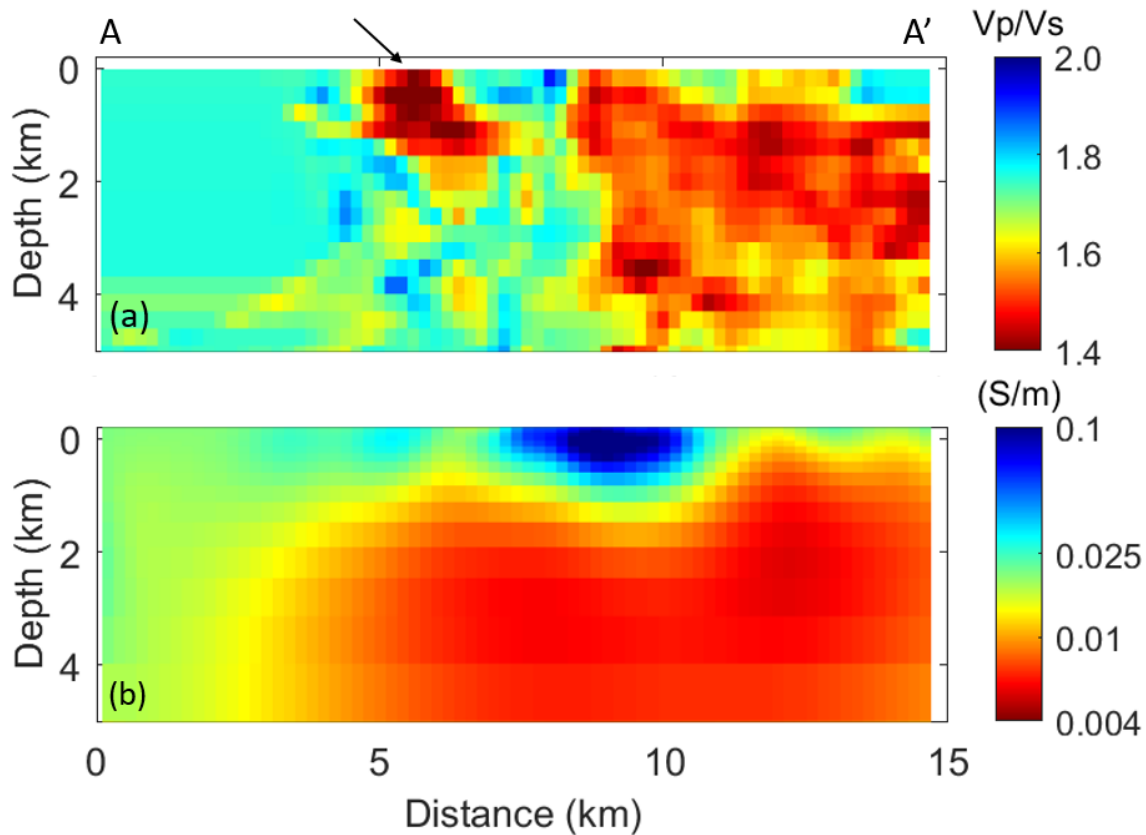
**Map showing the permanent seismic network (green triangles), the temporary seismic network (red triangles), and MT stations (yellow crosses) at The Geysers geothermal reservoir. Profiles A-A' and A-A'' denote the location of the cross sections discussed below.**

Source: Gritto et al., 2024

### Single-Physics Inversion

Before the joint inversion results are discussed, the single-physics seismic inversion images are compared to the single-physics MT images along the short profile A-A' (Figure 14) for data collected in 2021. While low electrical conductivity correlates to steam-filled regions or dry host rocks, it is difficult to spatially match low conductivity regions to low Vp/Vs regions, because of low resolution of the MT images. For example, the shallow steam reservoir (denoted by the black arrow in Figure 15) would not be confidently identified on profile A-A' of the conductivity model in Figure 15b without comparing the conductivity model against the corresponding Vp/Vs model.

**Figure 15: Cross Sections of  $V_p/V_s$  and Electrical Conductivity After Single Inversion**



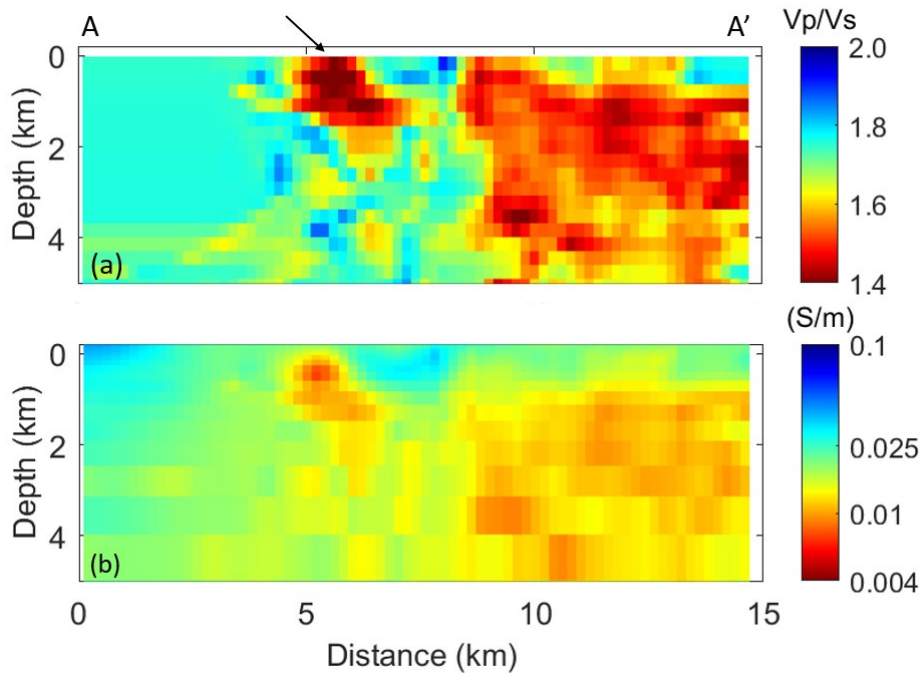
**Cross-sectional views of a standalone  $V_p/V_s$  model (top) and a standalone MT conductivity model (bottom) for data collected in 2021 along profile A-A' in Figure 14.**

Source: Gritto et al., 2024

### Multiple-Physics Inversion

After completing the joint inversion of seismic and MT data collected in 2021, the resulting  $V_p/V_s$  and electrical conductivity models are displayed in Figure 16. The joint inversion not only enhances the consistency between MT and seismic images but also introduces more detailed structures to the MT images. For example, the shallow low-conductivity steam reservoir (indicated by the black arrow) is clearly identified, with its dipping trend matching the seismic image. Additionally, on the right side, the deep low-conductivity structures closely resemble low  $V_p/V_s$  structures found in the corresponding regions of the seismic model (Figure 15a), both in terms of geometry and attribute magnitude.

**Figure 16: Cross Sections of Vp/Vs and Electrical Conductivity After Joint Inversion**



**Cross-sectional views of the joint inversion results: (a) the Vp/Vs model, and (b) the MT conductivity model, for data collected in 2021 along profile A-A' in Figure 14.**

Source: Gritto et al., 2024

On the other hand, it is notable that the joint inversion did not yield substantial improvement in the seismic inversion, as evident in Figures 15a and 16a. This observation can be explained by the fact that the MT survey is based on source fields and receivers being located outside the reservoir; this produces much lower resolution conductivity images compared to the seismic survey, which is based on earthquakes located within the reservoir, producing increased resolution. As a result, the MT images lack the structural details required to enhance the seismic inversion. However, because the MT images are derived from disparate data, they can be used to increase confidence in the interpretation of the seismic inversion images and in the interpretation of geophysical images that help operators to evaluate their reservoir management and to better understand their use of the geothermal resource including water injection, steam production, and well-planning operations.

### **Time-Lapse Multi-Physics Inversion**

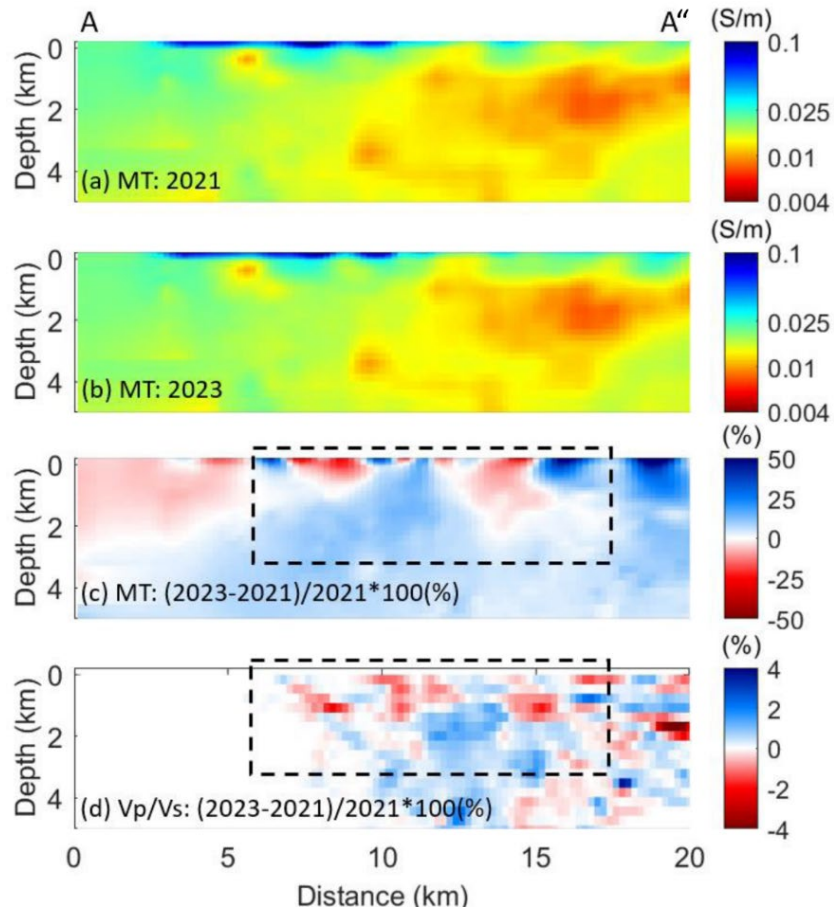
In this section, the joint inversion region is expanded to cover the entire area of The Geysers geothermal field and the results are presented along the longer profile A-A'' in Figure 14.

Below, MT images from joint seismic and MT inversions for the years 2021 and 2023 are presented along with their difference plots. Cross-sectional views along profile A-A'' of the joint MT inversion models for 2021 and 2023 are shown in Figure 17a and Figure 17b, respectively. The conductivity structures observed in these joint MT inversion models exhibit a considerable degree of correlation with those present in their corresponding Vp/Vs models (Appendix B, Figure B-1).

Figure 17c displays the relative differences in the joint MT inversion models for the two years, providing a visual representation of changes in conductivity. To facilitate a direct comparison, the relative difference in the corresponding Vp/Vs models over the same two-year interval are presented in Figure 17d. Overall, the correlation between the two relative difference plots is lower compared to the correlations between the Vp/Vs model and the joint MT inversion model in Figure 16. However, it is noteworthy that a consistent degree of similarity between the two types of difference plots is observed in the central region, denoted by the dashed rectangle. This limitation primarily results from the requirement for shared earthquake locations and ray paths in seismic time-lapse analysis, constraining the extent of the resolved Vp/Vs structure to the central region of the reservoir (Appendix A). The correlation between the two types of difference plots suggests that, within this central region, interpretations regarding changes within the reservoir can be made with greater confidence.

An interpretation of the single inversion and the joint inversion results is presented in the next section.

**Figure 17: Cross Sections of Electrical Conductivity and Vp/Vs After Joint Inversion**



**Cross-sectional views of the joint inversion results along profile A-A'' in Figure 14: (a) the MT conductivity model for 2021, (b) the MT conductivity model for 2023, (c) temporal changes in conductivity, and (d) temporal changes in Vp/Vs.**

Source: Gritto et al., 2024

# **Appraising Geophysical Data Through Geothermal Reservoir Model**

## **Appraising Spatio-temporal Vp/Vs Results**

In this section, the spatio-temporal correlations of Vp/Vs with water injection volumes and steam production throughout The Geysers are presented. The 3D volume of the temporal changes in Vp/Vs, presented in Chapter 3, "Passive Seismic Data Acquisition and Processing," and Appendix A, was incorporated in the 3D reservoir model to facilitate the appraisal of the spatial and temporal correlation to reservoir operations. Figure 18 shows a map view of the reservoir at a 5,000-foot depth, displaying the changes in Vp/Vs in percent between 2018.2019 and 2023. In the following section, all temporal changes in Vp/Vs are displayed in percentage. Superimposed are the volumes for several water injection wells, denoted by the blue discs. The size of the discs is proportional to the injected water volume from January 1, 2020, to April 30, 2023.

Two parallel faults, the Caldwell Ranch Fault and the Caldwell Pines Fault, indicated by the thick black lines, encompass an area of negative change in the Vp/Vs ratio, which may indicate an increase of steam concentration over the 3.5-year observation period. The clear delineation of high and low Vp/Vs ratios across these faults appears to support previous interpretations of reduced fault-permeability with respect to water and steam migration in this region (Hartline et al., 2015, 2016, 2019a).

Positive temporal Vp/Vs changes are co-located with major water injectors throughout The Geysers, which suggest an increase in water saturation in the vicinity of the injection wells. The highest Vp/Vs changes are found in the vicinity of boreholes OS-15, the largest water injector by volume, and Prati-15, where water injection started in January 2020. A closer look at the region surrounding the two wells is presented in Figure 19, which shows the temporal changes in Vp/Vs by colored dots, the locations of OS-15 and Prati-15, and contour lines representing the flow direction of injected water from tracer tests performed in Prati-15.

**Figure 18: Map of The Geysers With Water Injectors and Temporal Changes in Vp/Vs**

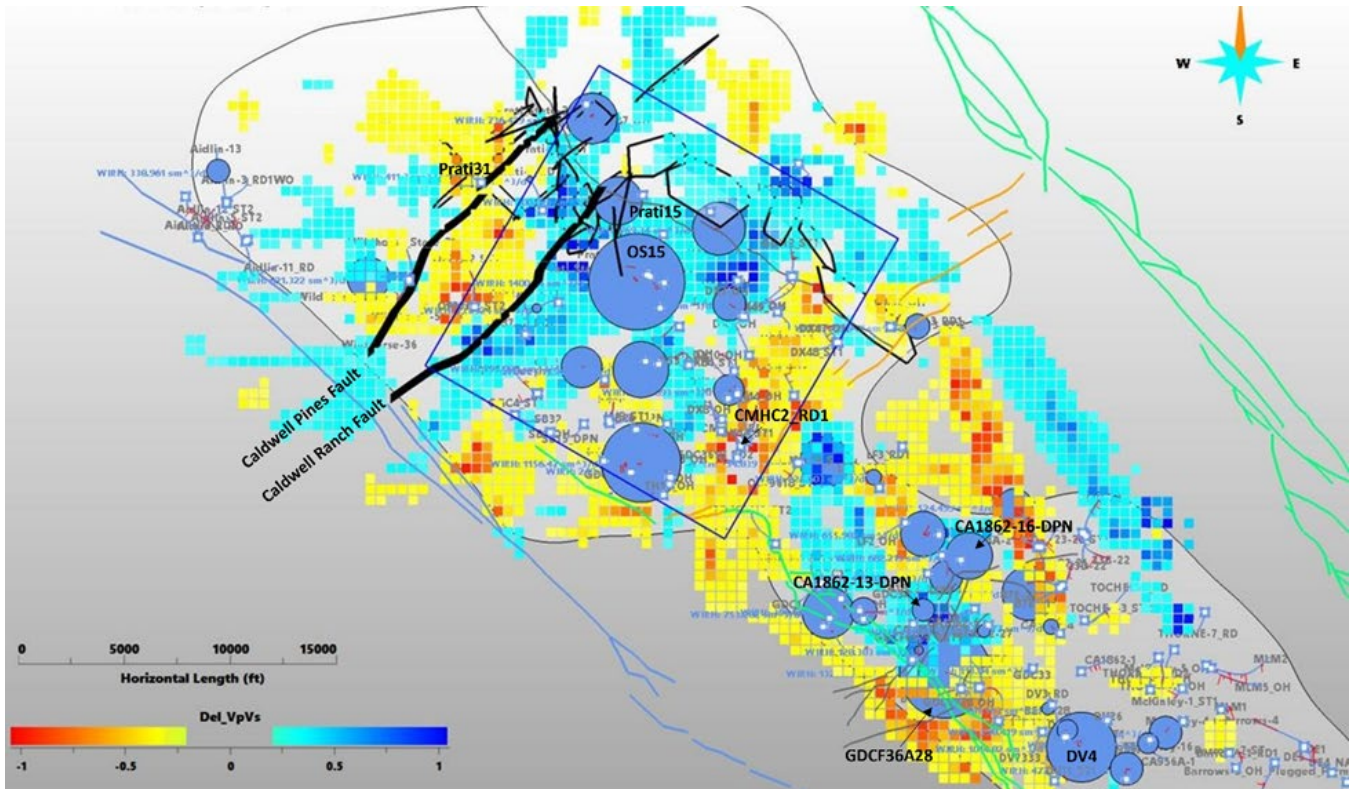
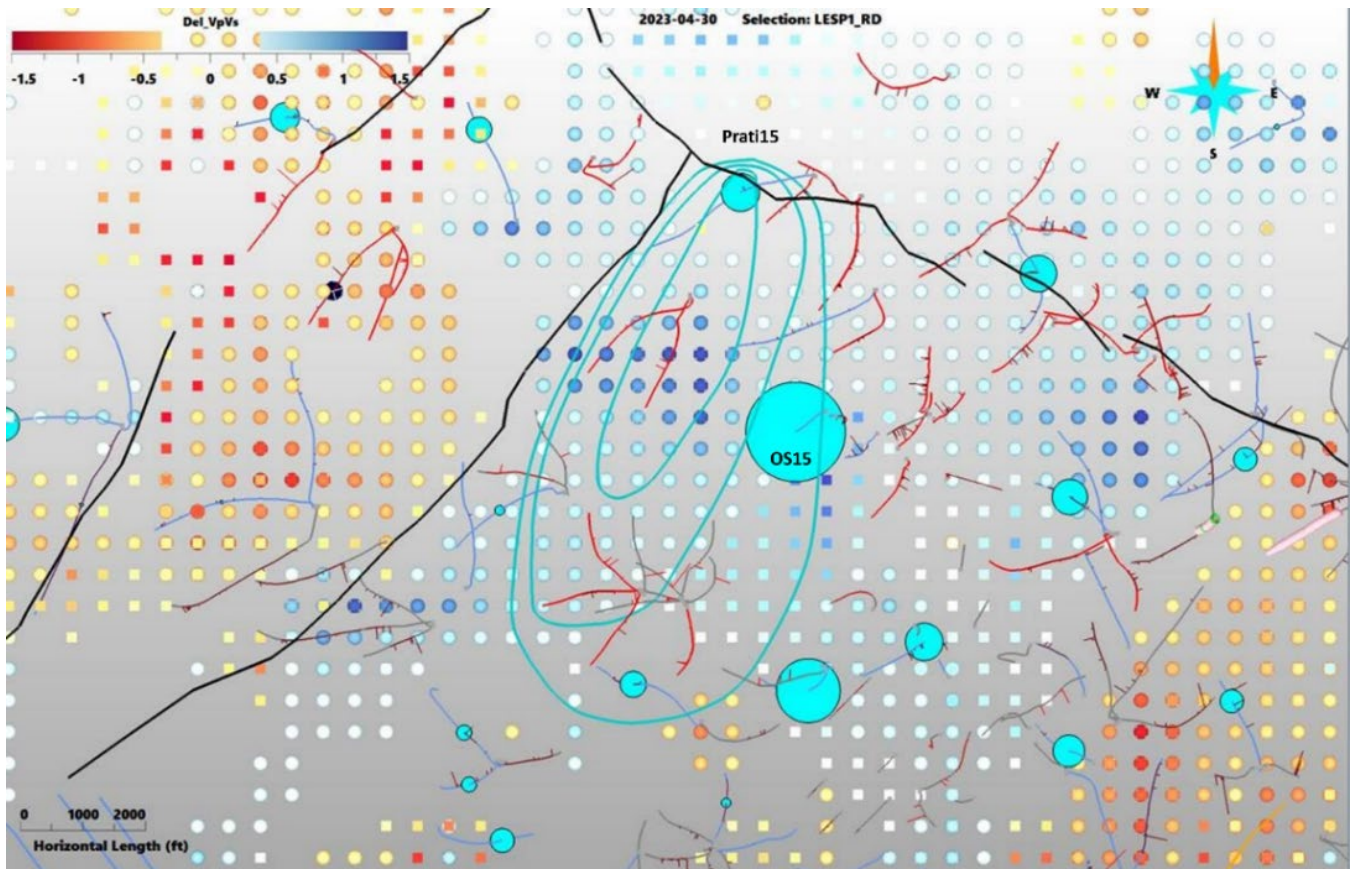


**Figure 19: Map of The Geysers With Water Injectors and Temporal Changes in Vp/Vs**



**Map of the northwest Geysers with water injectors OS-15 and Prati-15 and temporal changes in the Vp/Vs ratio calculated between the baseline of 2018.2019 and 2023 (colored pixels). The blue contour lines represent the results of tracer tests in Prati-15 and show the orientation of water flow at this reservoir horizon.**

Source: Gritto et al., 2024

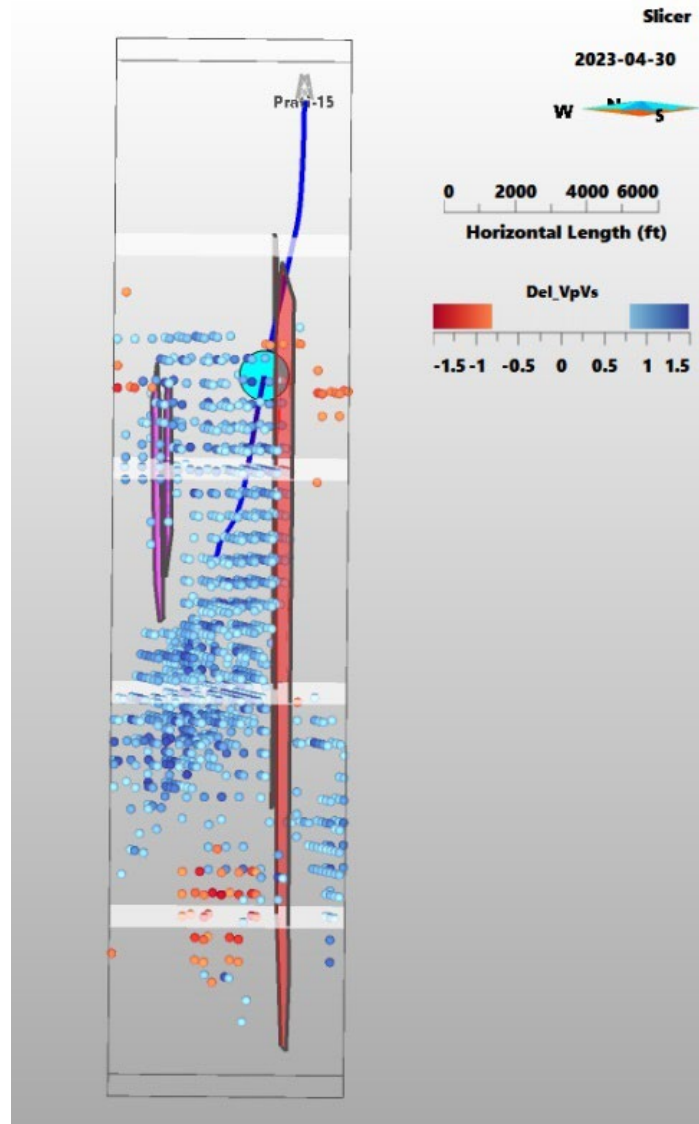
The highest positive anomalies in Vp/Vs are located in the center of the contour lines and to the west of water injector OS-15. The main flow direction of OS-15 was westward, as determined from the hypocenter pattern of induced seismicity (Hartline, 2023). The spatial correlation of high Vp/Vs changes and inferred flow pattern of these two water injectors suggest that the seismic data correctly predicted an increase in water saturation during the observation period.

The effect of faults on injected water volumes has been extensively reported by Hartline et al. (2015, 2016, 2019a). Throughout The Geysers, zones with isolated compartments bounded by impenetrable faults, which constitute hydraulic discontinuities, are encountered. Such a zone is displayed in Figure 20, which shows a 3D plot of the Prati-15 injection zone viewed from south-southwest. After the start of water injection in January 2020, the team expected the region below Prati-15 to experience a significant Vp/Vs change due to water injection into a rock volume with very limited previous water recharge. This temporal change in Vp/Vs is clearly visible in Figure 20, as is the inhibiting effect of the vertical faults on flow in lateral direction. It appears that the orange-colored fault to the east inhibits lateral flow down to a



depth of 10,000 feet, while the magenta-colored fault to the west inhibits flow where it is defined, while allowing flow in a westerly direction at greater depth. The concentration of negative temporal changes in  $V_p/V_s$  around a depth of 15,000 feet may indicate the conversion of water to steam in the deep and high-temperature part of the reservoir.

**Figure 20: Vertical View of Temporal Changes in  $V_p/V_s$  in Vicinity of the Prati-15 in the Northwest Geysers**



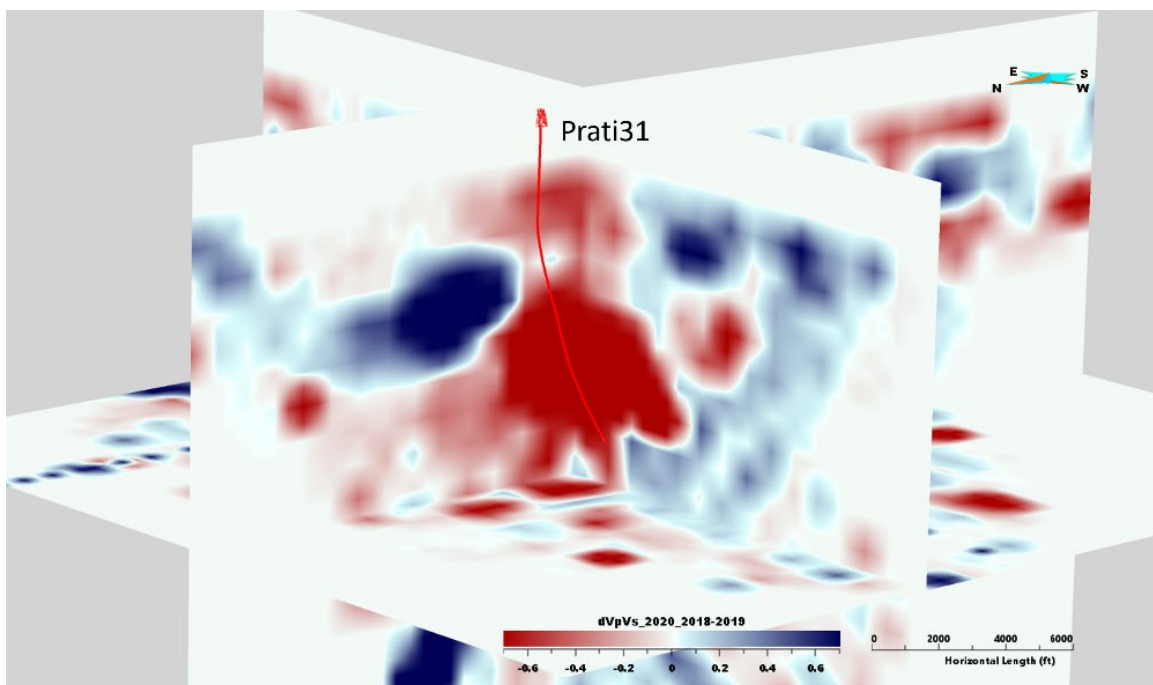
**View of the temporal changes in  $V_p/V_s$  in percent between 2018-2019 and 2023 (colored dots) in the vicinity of Prati-15 (blue trajectory). The center of water injection is denoted by the blue disc. Vertical fault surfaces inhibit the water flow to either side. The white horizontal surfaces represent slices at depths of 0, 5,000, 10,000, and 15,000 feet.**

Source: Gritto et al., 2024

While the examples above successfully demonstrated the use of positive temporal changes in  $V_p/V_s$  to delineate an increase of water saturation in the reservoir, the following example illustrates how negative temporal changes in  $V_p/V_s$  can be used to delineate increases in steam concentration.

A high-temperature EGS was established in the northwest Geysers in 2012, with steam production commencing in 2017 (Hartline et al., 2019b). Steam production during the first two years was minimal, but it ramped up in 2019 and 2020 (Hartline, 2023), which led to an increase in steam volume in 2020 relative to 2018.2019. That increase in steam volume is reflected in Figure 21 by the negative Vp/Vs change indicated by the red color in the vicinity of the steam producer Prati-31.

**Figure 21: Temporal Changes of Vp/Vs for Steam Producer Prati-31 in the Northwest Geysers**



**Fence diagram with steam producer Prati-31 and temporal Vp/Vs changes between 2018.2019 and 2020, located in the northwest Geysers.**

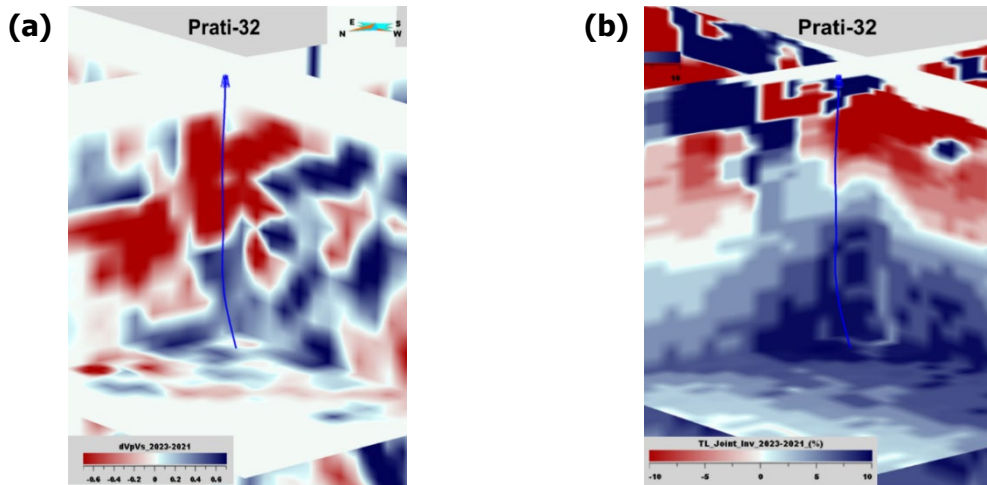
Source: Gritto et al., 2024

### **Appraising Spatio-temporal Vp/Vs and Electrical Conductivity Results**

In Chapter 3, “Joint Inversion of Multiphysics Data,” the results of joint inversions of seismic and MT data were presented to show how this approach increases the confidence in the location of water and steam concentrations over the single-physics data inversion. In this section, the results of joint inversions of seismic and MT data are shown and compared to single-physics seismic inversion results. Because MT surveys were conducted in 2021, 2022, and 2023, time-lapse data between 2021 and 2023 were selected, as they offer the opportunity to observe stronger temporal changes in the reservoir.

The first example is based on the EGS water injector Prati 32 in the northwest Geysers, for which temporal changes between 2021 and 2023 in Vp/Vs and electrical conductivity are shown in Figure 22. Both results show an increase in Vp/Vs and electrical conductivity in the lower half of the wells where the water injection was taking place. Considering continuous water injection in Prati-32 between 2021 and 2023, these results appear to confirm the accumulation of a water plume at depth.

**Figure 22: Temporal Changes in Vp/Vs and Electrical Conductivity for Water Injector Prati-32 in the Northwest Geysers**

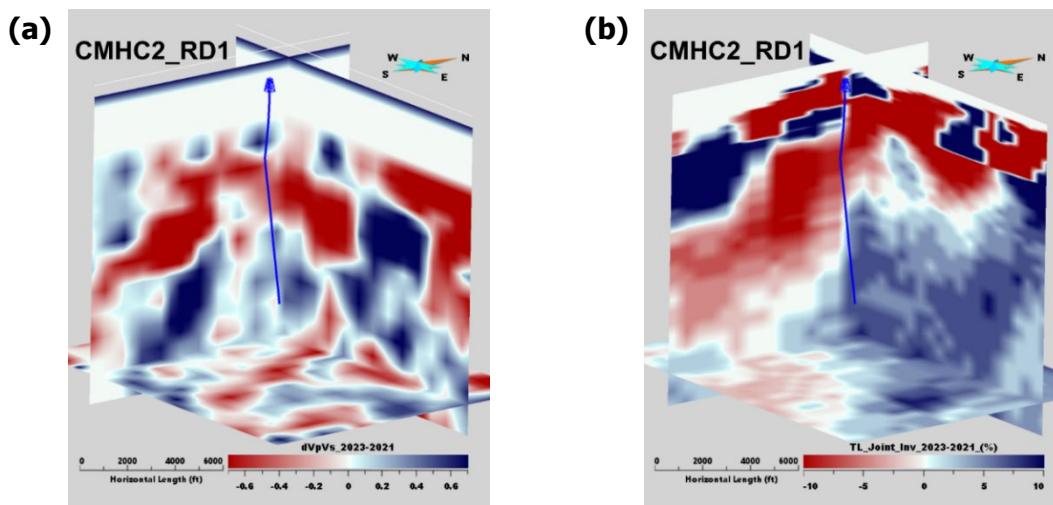


**Fence diagram of seismic and MT data in the vicinity of water injection well Prati-32 in the northwest Geysers: (a) temporal changes in Vp/Vs in percent between 2021 and 2023, and (b) temporal changes in electrical conductivity in percent resulting from joint inversion of seismic and MT data between 2021 and 2023.**

Source: Gritto et al., 2024

Water injection is also ongoing in the central Geysers, where the trajectory of injector CMHC2\_RD1 is indicated by the blue trajectory in Figure 23. Figure 23a displays temporal changes in Vp/Vs for the period from 2021 to 2023, while Figure 23b shows the change in electrical conductivity during the same location period. The borehole is tapping into an area of positive Vp/Vs ratio and positive electrical conductivity, which suggests an increase in water concentration during the two-year period.

**Figure 23: Temporal Changes in Vp/Vs and Electrical Conductivity for Water Injector CMHC2\_RD1 in the Central Geysers**



**Fence diagram of seismic and MT data in the vicinity of water injection well CMHC2\_RD1 in the central Geysers: (a) temporal changes in Vp/Vs in percent between 2021 and 2023, and (b) temporal changes in electrical conductivity in percent resulting from joint inversion of seismic and MT data between 2021 and 2023.**

Source: Gritto et al., 2024

# CHAPTER 4:

## Conclusion

---

The primary goal of the current project included the development of geophysical imaging techniques using seismic and MT data to jointly image structural features and dynamic properties at The Geysers steam field to support geothermal energy generation. The technical advancements of this project were provided by monitoring time-lapse changes in both seismic velocity and electrical conductivity that occur in the reservoir due to water injection and steam production, and by the joint inversion of the multi-physics (seismic and MT) data, which provided images of the reservoir structure with higher confidence than either of the data sets by themselves. Ultimately, these images can be used for improved estimation of reservoir heterogeneities and spatial distributions of water and steam at depth, for enhanced reservoir monitoring, and for more accurate placement of injection and production wells.

Specifically, the seismic imaging of the Vp/Vs distribution in the reservoir yielded high spatio-temporal correlations with field data derived from borehole observations from hundreds of wells in The Geysers reservoir. High and low Vp/Vs ratios correlated with water and steam-saturated zones, respectively, providing a better understanding for the physical processes in regions away from and between boreholes. This was corroborated by MT data in the form of electrical conductivity, which indicated regions with water (high electrical conductivity) and steam (low electrical conductivity) concentrations. The joint inversion of seismic and MT data supported the findings of the single-physics data, and it yielded results that improved the spatial resolution of the MT data while increasing the confidence of the seismic imaging results.

The results of the project add confidence in the development of the 3D reservoir model, which forms the basis for reservoir management, such as well-planning and siting. Knowing the spatial distribution of water and steam reduces the danger of drilling dry holes. Drilling costs of boreholes range from \$7.0 million for wells of 8,500 feet in length to \$8.3 million for wells of 10,000 feet in length. In the current case, the cost savings for the California rate payer can be substantial, considering that the project covered about 80 percent of The Geysers steam field, with several hundred boreholes.

The results of the project also support the continued management of the resource at The Geysers, assuring the sustained viability of the resource in the future. Geothermal energy is clean, has a small environmental footprint, and is available 24 hours per day. It is independent of sunlight or wind speed, unlike solar installations or wind turbines. Therefore, geothermal energy adds a reliable source to California's green energy portfolio.

The application of the developed technique to other geothermal reservoirs is straightforward. Because the seismic method is passive, the cost of data acquisition is low, resulting from the use of recently developed inexpensive recording stations (Gritto and Nakagawa, 2020) and automated data processing techniques (Gritto, 2023). Furthermore, MT surveys can be acquired by a small crew in one to two weeks, depending on the size of the reservoir, which minimizes acquisition cost. As such, the technology can be applied to other geothermal

reservoirs in California, such as the Coso or the Salton Sea geothermal field, or to other geothermal reservoirs in the United States, including the Basin and Range region, as long as natural or induced seismicity through water injection is observed. It is noted that, in regions where the rate of seismicity is lower than at The Geysers, MT data might help to provide higher resolution in the  $V_p/V_s$  images.

The lower resolution of MT data compared to seismic data limits the utility of the resulting electric conductivity images to increasing the confidence in the seismic results rather than improving the resolution of the joint multi-physics images. This can be improved by jointly acquiring and inverting MT data and controlled source electromagnetic (CSEM) data. CSEM data can be acquired using a limited number of grounded electric dipole sources, keeping data acquisition costs low. The joint inversion of MT and CSEM data not only ensures imaging depths that effectively cover geothermal reservoirs but also enhances resolution. Thus, the combination of passive seismic, MT, and CSEM imaging should be investigated in a future study.

## GLOSSARY AND LIST OF ACRONYMS

Term	Definition
3D	three-dimensional
bit	the smallest unit of information in a computer, defined by either 0 or 1
Calpine	Calpine Corporation
CEC	California Energy Commission
cm	centimeters
CSEM	controlled source electromagnetic
DWS	derivative weight sum
EGS	enhanced geothermal system
Felsite	a granitic rock that intruded the base of The Geysers reservoir millions of years ago and is assumed to be the heat source for the region
GaMMA	Gaussian Mixture Model Association
GPS	Global Positioning System
Graywacke	a metamorphosed sandstone
Greenstone	a generic term for green-hued minerals and metamorphosed igneous rock
GTO	Geothermal Technology Office (U.S. DOE)
GW	gigawatt
Hornfelsic graywacke	a mixture of rock types consisting of hornfels and metamorphosed sandstone that comprise the majority of The Geysers geothermal reservoir rock
Hz	hertz
km, km <sup>2</sup>	kilometer, square kilometer
LAN	local area network
m	meter
MT	magnetotelluric
MW	megawatt
NE	northeast
$\Omega$ m	Ohm meter is the unit of electrical resistivity
raypath	line that shows the direction the seismic wave is propagating
S-m, S/m	Siemens per meter
Sandstone	A sedimentary rock
SB	Senate Bill

Term	Definition
SD	secure digital
Serpentinite	a green-colored rock composed predominantly of one or more serpentine group minerals
sps	samples per second
SW	southwest
U.S. DOE	United States Department of Energy
VDC	volt direct current
Vp	P-wave velocity
Vp/Vs	ratio of seismic P-wave to S-wave propagation velocities
Vs	S-wave velocity
W	watt

# References

---

- Boitnott, G.N., and A. Kirkpatrick. 1997. "Interpretation of Field Seismic Tomography at The Geysers Geothermal Field, California." *PROCEEDINGS, Twenty-Second Workshop on Geothermal Reservoir Engineering*, Stanford University, Stanford, California. January 27-29, 1997. Contract Number SGP-TR-155. Available at <https://www.researchgate.net/publication/237472103> *Interpretation of Field Seismic Tomography at The Geysers Geothermal Field California*.
- Caldwell, T.G., H.M. Bibby, and C. Brown. 2004. "The magnetotelluric phase tensor." *Geophysical Journal International*, 158(2), 457–469. Available at <https://doi.org/10.1111/j.1365-246x.2004.02281.x>.
- Chave, A., and A. Jones (eds.). 2012. *The Magnetotelluric Method: Theory and Practice*. Cambridge: Cambridge University Press. Available at <https://doi.org/10.1017/CBO9781139020138>.
- Egbert, G.D, and J.R. Booker. 1986. "Robust estimation of geomagnetic transfer functions." *Geophysical Journal of the Royal Astronomical Society*, 87(1), 173–194. Available at <https://doi.org/10.1111/j.1365-246X.1986.tb04552.x>.
- Egbert, G.D., and A. Kelbert. 2012. "Computational recipes for electromagnetic inverse problems." *Geophysical Journal International*, 189(1), 251–267. Available at <http://doi.org/10.1111/j.1365-246x.2011.05347.x>.
- Gallardo, L.A., and M.A. Meju. 2003. "Characterization of heterogeneous near-surface materials by joint 2D inversion of dc resistivity and seismic data." *Geophysical Research Letters*, 30(13), 1658. Available at <http://doi.org/10.1029/2003GL017370>.
- Gallardo, L., and M. Meju. 2007. "Joint two-dimensional cross-gradient imaging of magnetotelluric and seismic travelttime data for structural and lithological classification." *Geophysical Journal International*, 169, 1261–1272. Available at <http://doi.org/10.1111/j.1365-246X.2007.03366.x>.
- Gritto, R., T.M. Daley, and L.R. Myer. 2004. "Joint Cross-Well and Single-Well Seismic Studies of CO<sub>2</sub> Injection in an Oil Reservoir." *Geophysical Prospecting*, 52(4), 323–339. Available at <https://doi.org/10.1111/j.1365-2478.2004.00418.x>.
- Gritto, R., S.H. Yoo, and S.P. Jarpe. 2013a. "Three-dimensional seismic tomography at The Geysers geothermal field, CA, USA." *PROCEEDINGS, 38th Workshop on Geothermal Reservoir Engineering*, Stanford University, Stanford, California. February 11–13, 2013. Contract Number SGP-TR-198. Available at <https://pangea.stanford.edu/ERE/pdf/IGAstandard/SGW/2013/Gritto.pdf>.
- Gritto, R., S.H. Yoo, and S.P. Jarpe. 2013b. "Seismic Imaging of Reservoir Structure at The Geysers Geothermal Reservoir." *PROCEEDINGS, American Geophysical Union Fall Meeting*, S33D-2460, San Francisco, USA. December 9–13, 2013. Available at <https://ui.adsabs.harvard.edu/abs/2013AGUFM.S33D2460G/abstract>.



- Gritto, R., and S.P. Jarpe. 2014. "Temporal variations of Vp/Vs-ratio at The Geysers geothermal field, USA." *Geothermics*, 52, 112–119. Available at <https://doi.org/10.1016/j.geothermics.2014.01.012>.
- Gritto, R., and S. Nakagawa. 2020. *High-Resolution Imaging of Geothermal Flow Paths Using a Cost-Effective Dense Seismic Network*. Final Project Report, 1-48. California Energy Commission. Contract Number EPC-16-021. Available at <https://www.energy.ca.gov/sites/default/files/2021-05/CEC-500-2021-004.pdf>.
- Gritto R., S.P. Jarpe, C. Hartline, and C. Ulrich. 2023. "Seismic Imaging of Reservoir Heterogeneity Using a Network with High Station Density at The Geysers Geothermal Reservoir, CA, USA." *Geophysics*, 88(5), WB11-WB22. Available at <https://pubs.geoscienceworld.org/geophysics/article-abstract/88/5/WB11/623996/Seismic-imaging-of-reservoir-heterogeneity-using-a>.
- Gritto R. 2023. *Task 2: Passive Seismic Data Acquisition and Processing*. Report 3. California Energy Commission. Contract Number EPC-19-019.
- Gritto, R., E.S. Um, J. Peacock, S.P. Jarpe, C. Ulrich, C.S. Hartline, and D.L. Alumbaugh. 2024. *Joint Time-Lapse Acquisition and Inversion of Passive Seismic and Magnetotelluric Data for Monitoring Reservoir Processes at The Geysers Geothermal Field*. California Energy Commission. Publication Number: CEC-500-2024-075.
- Haber, E., and D. Oldenburg. 1997. "Joint inversion: a structural approach." *Inverse Problems*, 13(1), 63–77. Available at <https://doi.org/10.1088/0266-5611/13/1/006>.
- Harris, P., and L. MacGregor. 2006. "Determination of reservoir properties from the integration of CSEM, seismic, and well-log data." *First Break*, 24(11), 53–59. Available at <https://doi.org/10.3997/1365-2397.24.11.27178>.
- Hartline, C.S. 2023. Personal communication.
- Hartline, C.S., M.A. Walters, M.C. Wright, C.K. Forson, and A.J. Sadowski. 2015. "Three-dimensional structural model building, induced seismicity analysis, drilling analysis, and reservoir management at The Geysers geothermal field, Northern California." *GRC Transactions*, 39, 603–614. Geothermal Resource Council.
- Hartline, C.S., M.A. Walters, M.C. Wright, C.K. Forson, and A.J. Sadowski. 2016. "Three-Dimensional Structural Model Building, Induced Seismicity Analysis, Drilling Analysis and Reservoir Management at The Geysers Geothermal Field, Northern California." *PROCEEDINGS, 41st Workshop on Geothermal Reservoir Engineering*, Stanford University, Stanford, California. February 22-24, 2016. Contract Number SGP-TR-209, 12.
- Hartline, C.S., M.A. Walters, and M.C. Wright. 2019a. "Three-Dimensional Structural Model Building Constrained by Induced Seismicity Alignments at The Geysers Geothermal Field, Northern California." *GRC Transactions*, 43, 24. Geothermal Resource Council.
- Hartline, C.S., M.A. Walters, M.C. Wright, C. Rawal, J. Garcia, and J. Farison. 2019b. *The Northwest Geysers Enhanced Geothermal System Demonstration Project, The Geysers, California*. Final Report. Office of Scientific and Technical Information, United States Department of Energy. Available at <https://doi.org/10.2172/1523288>.

- Hoversten, G., F. Cassassuce, E. Gasperikova, G. Newman, J. Chen, Y. Rubin, Z. Hou, and D. Vasco. 2006. "Direct reservoir parameter estimation using joint inversion of marine seismic AVA and CSEM data." *Geophysics*, 71(3), C1–C13. Available at <https://doi.org/10.1190/1.2194510>.
- MIT Energy Initiative. 2006. *The Future of Geothermal Energy: Impact of Enhanced Geothermal Systems (EGS) on the United States in the 21<sup>st</sup> Century*. Massachusetts Institute of Technology Energy Initiative. ISBN:0-615-11746. Available at <https://energy.mit.edu/research/future-geothermal-energy/>.
- Peacock, J.R., S. Thiel, P. Reid, and G. Heinson. 2012. "Magnetotelluric monitoring of a fluid injection: Example from an enhanced geothermal system." *Geophysical Research Letters*, 39(18). Available at <https://doi.org/10.1029/2012gl053080>.
- Peacock, J.R., S. Thiel, G.S. Heinson, and P. Reid. 2013. "Time-lapse magnetotelluric monitoring of an enhanced geothermal system." *Geophysics*, 78(3), B121–B130. Available at <https://doi.org/10.1190/geo2012-0275.1>.
- Peacock, J.R., M.T. Mangan, D. McPhee, and D.A. Ponce. 2015. "Imaging the magmatic system of Mono Basin, California, with magnetotellurics in three dimensions." *Journal of Geophysical Research: Solid Earth*, 120(11), 7273–7289. Available at <https://doi.org/10.1002/2015JB012071>.
- Peacock, J.R., M.T. Mangan, M. Walters, C. Hartline, J. Glen, T.E. Earney, and W.D. Schermerhorn. 2019. "Geophysical Characterization of the heat source in the Northwest Geysers, California." *PROCEEDINGS, 44th Workshop on Geothermal Reservoir Engineering*, Stanford University, Stanford, California. February 11-13, 2019. Contract Number SGP-TR-214. Available at <https://pangea.stanford.edu/ERE/db/GeoConf/papers/SGW/2019/Peacock.pdf>.
- Peacock, J., T. Earney, M. Mangan, W. Schermerhorn, J. Glen, M. Walters, and C. Hartline. 2020. "Geophysical characterization of the Northwest Geysers geothermal field, California." *Journal of Volcanology and Geothermal Research*, 399, 106882. Available at <https://doi.org/10.1016/j.jvolgeores.2020.106882>.
- Um, E.S., M. Commer, and G.A. Newman. 2014. "A strategy for coupled 3D imaging of large-scale seismic and electromagnetic data sets: Application to subsalt imaging." *Geophysics*, 79(3), ID1-ID13. Available at <https://doi.org/10.1190/geo2013-0053.1>.
- Um, E.S., M. Commer, R. Gritto, J.R. Peacock, D.L. Alumbaugh, S.P. Jarpe, and C. Hartline. 2023. "Cooperative Joint Inversion of Magnetotelluric and Microseismic Data for Imaging The Geysers Geothermal Field, California, USA." *Geophysics*, 88.(5), WB45–WB54. Available at <https://doi.org/10.1190/GEO2022-0521.1>.
- Zhang, H., and C. Thurber. 2003. "Double-difference tomography: The method and its application to the Hayward Fault, California." *Bulletin of the Seismological Society of America*, 93(5), 1875-1889. Available at <https://doi.org/10.1785/0120020190>.

Zhu, W., and G.C. Beroza. 2019. "PhaseNet: A Deep-Neural-Network-Based Seismic Arrival-Time Picking Method." *Geophysical Journal International*, 216(1), 261–273. Available at <https://doi.org/10.1093/gji/ggy423>.

# Project Deliverables

---

Project deliverables, including interim project reports, are available upon request by submitting an email to [pubs@energy.ca.gov](mailto:pubs@energy.ca.gov).

- Task 2 Passive Seismic Data Acquisition and Processing, Reports 1–3
- Task 3 Magnetotelluric Data Acquisition and Processing, Reports 1–3
- Task 4 Joint Inversion of Magnetotelluric and Seismic Data, Report
- Task 5 Correlation Analysis of Geophysical Imaging and Reservoir Model, Report
- Final Report
- Final Fact Sheet
- Technology Transfer Report

The project produced several publications listed below:

Gritto, R., S.P. Jarpe, and D.L. Alumbaugh. 2022. "New Large-Scale Passive Seismic Monitoring at The Geysers Geothermal Reservoir, CA, USA." *PROCEEDINGS, 47th Workshop on Geothermal Reservoir Engineering*, Stanford University, Stanford, California. February 7-9, 2022. Contract Number SGP-TR-223. Available at <https://pangea.stanford.edu/ERE/db/GeoConf/papers/SGW/2022/Gritto.pdf>.

Peacock, J., D.L. Alumbaugh, C. Hartline, and M. Mitchell. 2022. "Repeat magnetotelluric measurements to monitor The Geysers steam field in northern California." *PROCEEDINGS, 47th Workshop on Geothermal Reservoir Engineering*, Stanford University, Stanford, California. February 7-9, 2022. Contract Number SGP-TR-223. Available at <https://pangea.stanford.edu/ERE/db/GeoConf/papers/SGW/2022/Peacock.pdf>.

Gritto, R., S.P. Jarpe, C. Hartline, and C. Ulrich. 2023. "Seismic Imaging of Reservoir Heterogeneity Using a Network with High Station Density at The Geysers Geothermal Reservoir, CA, USA." *Geophysics*, 88(5), WB11-WB22. Available at <https://doi.org/10.1190/geo2022-0490.1>.

Peacock, J., D.L. Alumbaugh, M. Mitchel, and C. Hartline. 2023. "Magnetotelluric Monitoring of The Geysers Steam Geothermal Field, Northern California: Phase 2." *PROCEEDINGS, 48th Workshop on Geothermal Reservoir Engineering*, Stanford University, Stanford, California. February 6-8, 2023. Contract Number SGP-TR-224. Available at <https://pubs.usgs.gov/publication/70245363>.

Um, E.S., M. Commer, R. Gritto, J.R. Peacock, D.L. Alumbaugh, S.P. Jarpe, and C. Hartline. 2023. "Cooperative Joint Inversion of Magnetotelluric and Microseismic Data for Imaging The Geysers Geothermal Field, California, USA." *Geophysics*, 88(5), WB45–WB54. Available at <https://doi.org/10.1190/GEO2022-0521.1>.

Peacock, J., D.L. Alumbaugh, M. Mitchel, and C. Hartline. 2024. "Summary of Annual Repeat Magnetotelluric Surveys of the Geysers Geothermal Field." *PROCEEDINGS, 49th Workshop on Geothermal Reservoir Engineering*, Stanford University, Stanford, California. February 12-14, 2024. Contract Number SGP-TR-225. Available at <https://pangea.stanford.edu/ERE/db/GeoConf/papers/SGW/2024/Peacock.pdf>.



**CALIFORNIA  
ENERGY COMMISSION**



**ENERGY RESEARCH AND DEVELOPMENT DIVISION**

# **Appendix A: Passive Seismic Imaging**

**June 2024 | CEC-500-2024-075**



# APPENDIX A:

## Passive Seismic Imaging

---

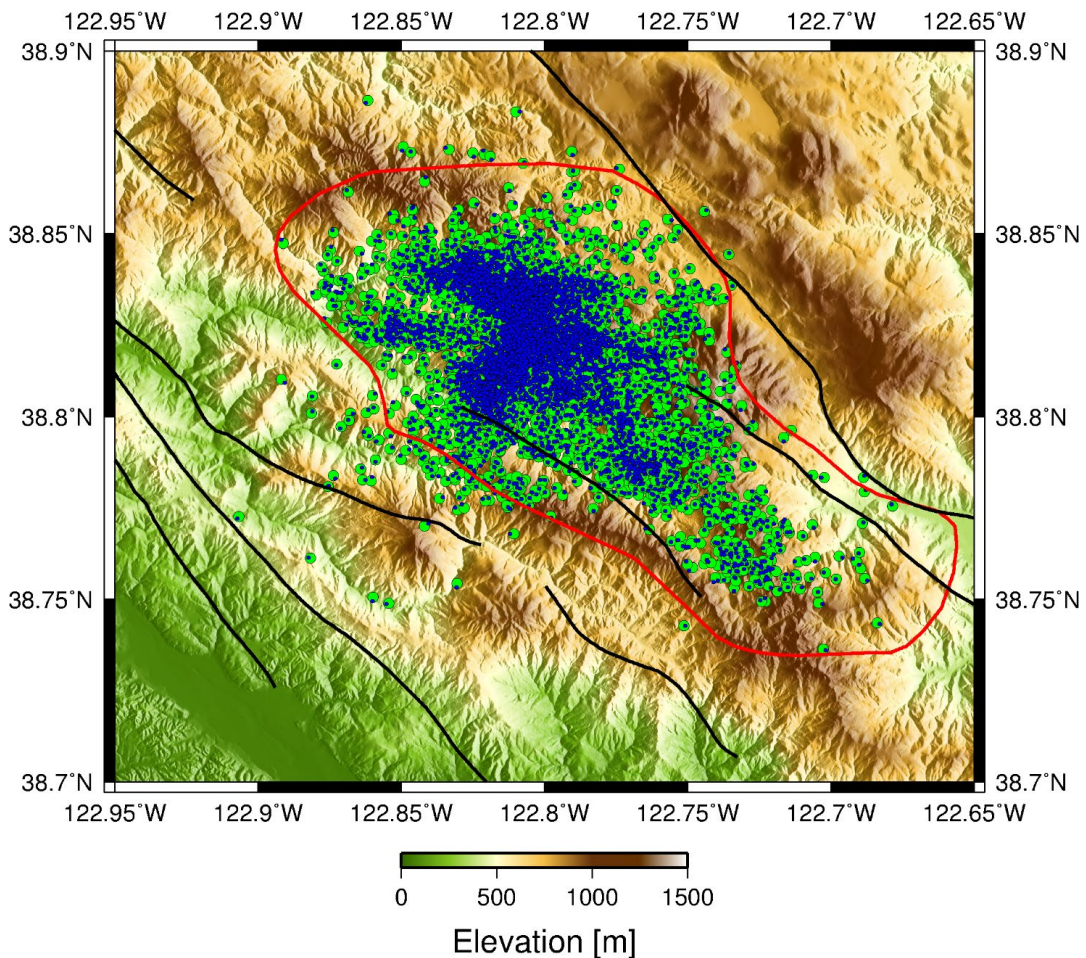
### Principles of Time-lapse Seismic Imaging

Knowledge of the temporal changes in the geothermal reservoir is important to optimize reservoir management and to better understand the use of the resource. Seismic tomographic imaging is based on the principle that travel times of seismic waves, observed at seismic stations, are inverted for the seismic velocity structure in the reservoir. This is done by using the principle of ray tracing, where the path of seismic waves from the earthquake hypocenter to the seismic station is considered. In principle, the travel time observed at the seismic station is back-projected along the raypath to the earthquake to compute the distribution of the seismic velocities along the ray. If this is done for a sufficiently high number of rays, a 3D velocity model of the subsurface can be constructed. However, if the velocity models derived from different datasets are compared, the problem arises that each dataset is based on a separate set of earthquake locations and therefore the associated raypaths to the seismic stations propagate through separate parts of the reservoir.

To address this problem, the team used the approach of Gritto et al. (2013b), which is based on (1) running the inversion for each dataset separately to invert for the 3D velocity structure and for hypocenter locations, and (2) selecting co-located earthquakes from each dataset. While a hard co-location requirement would likely result in zero events (i.e., no two events are ever exactly co-located), the requirement is softened to include all events that are co-located within a maximum distance of 150 meters. This limit is equivalent to one-half Fresnel zone of the S-wave wavelength at The Geysers. Therefore, when the S-waves propagate from neighboring events that are located within a distance of 150 meters to the same recording stations, their sensitivity kernels overlap while propagating through the reservoir and sensing the same structure. Because the wavelength of the P-wave is longer than that of the S-wave, their sensitivity kernels overlap even more. If in addition, only those P-phases and S-phases are selected that are recorded in both datasets at common stations, the result is two datasets with common raypaths propagating through the reservoir and sensing the same structure. If the parameterization of the inversion of the two datasets is identical, the resulting velocity models can be compared and differenced to appraise temporal changes in the medium.

The first spatio-temporal analysis was based on seismic data covering the period from June 2018 (the inception of the seismic CEC-network) to December 2019 (referred to in the following as the 2018.2019 seismic data), which served as the baseline measurement for the seismic analysis. The first temporal analysis paired the seismic results of the 2018.2019 data to the seismic results of 2020, using the data processing described in the previous paragraph. The search for co-located earthquakes from each dataset resulted in two sets of 6,300 events, which are presented in Figure A-1. The map shows the spatial distribution of earthquake epicenter locations, with the 2018.2019 events shown in green and the 2020 events shown in blue. The co-location of the events can be assessed by the close proximity of the epicenter pairs.

**Figure A-1: Map With Co-located Earthquakes From 2018.2019 and 2020**

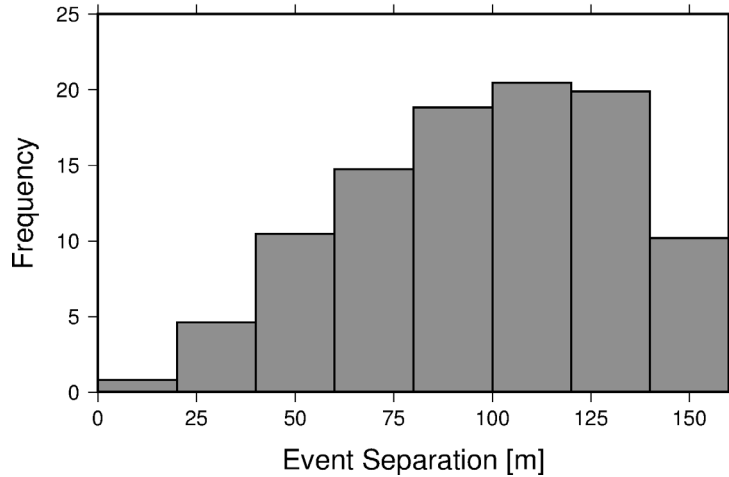


**Map of The Geysers geothermal reservoir, with the outline of the steam field shown by the red polygon, and surface traces of known faults in the region shown by the black lines. The 6,300 co-located events are denoted by the green circles (2018.2019 data) and the blue dots (2020 data).**

Source: Gritto et al., 2024

As explained above, the maximum allowable distance between the co-located events was set to 150 meters to ensure overlapping S-wave sensitivity kernels between the two different epochs. A histogram displaying the actual distribution of the distance between the two datasets is shown in Figure A-2. Most events have a separation distance of between 60 meters and 135 meters, much smaller than the maximum allowable threshold. Consequently, the sensitivity kernels overlap even more and the results between the two epochs can be well differentiated. With the co-located events selected, P-wave and S-wave phase arrivals from both datasets were matched, such that the seismic rays from the events to the common recording stations are covering the same region of the reservoir. The separate inversions were performed with the same parameterization (number of iterations, damping, weighting, misfit reduction, etc.) and the tomographic results subsequently differentiated. The results of the time-lapse seismic imaging are presented in the section of Chapter 3 titled "Passive Seismic Data Acquisition and Processing" and below.

**Figure A-2: Histogram of the Separation Distance Between Selected Earthquakes in 2018.2019 and 2020**



**Histogram of the separation distance between selected earthquakes in 2018.2019 and 2020. The majority of the selected earthquakes have separation distances between 60 and 135 meters.**

Source: Gritto et al., 2024

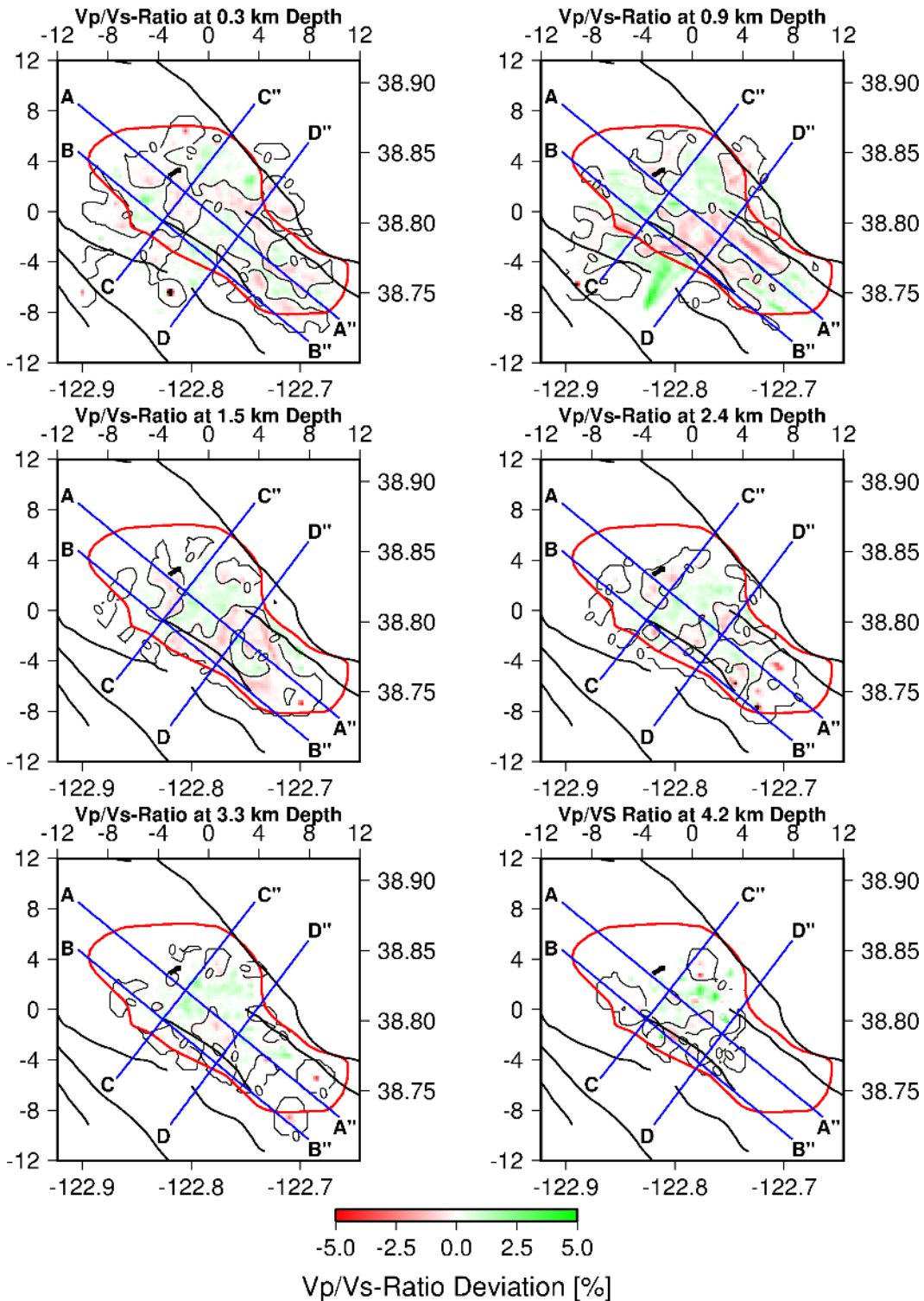
### **Time-lapse Imaging Between 2023 and 2018.2019**

The team also processed the seismic data from 2023 and 2018.2019 and computed the temporal changes between these two epochs.

The temporal changes in  $V_p/V_s$  are shown in Figure A-3, which displays horizontal sections through the reservoir. As before, results are plotted only for regions that have sufficient ray coverage as determined by the derivative weight sum (DWS). The magnitude of change is similar to that observed for the 2020-2018.2019 period, with the strongest changes in the upper reservoir.



**Figure A-3: Horizontal Slices of Temporal Changes in Vp/Vs**

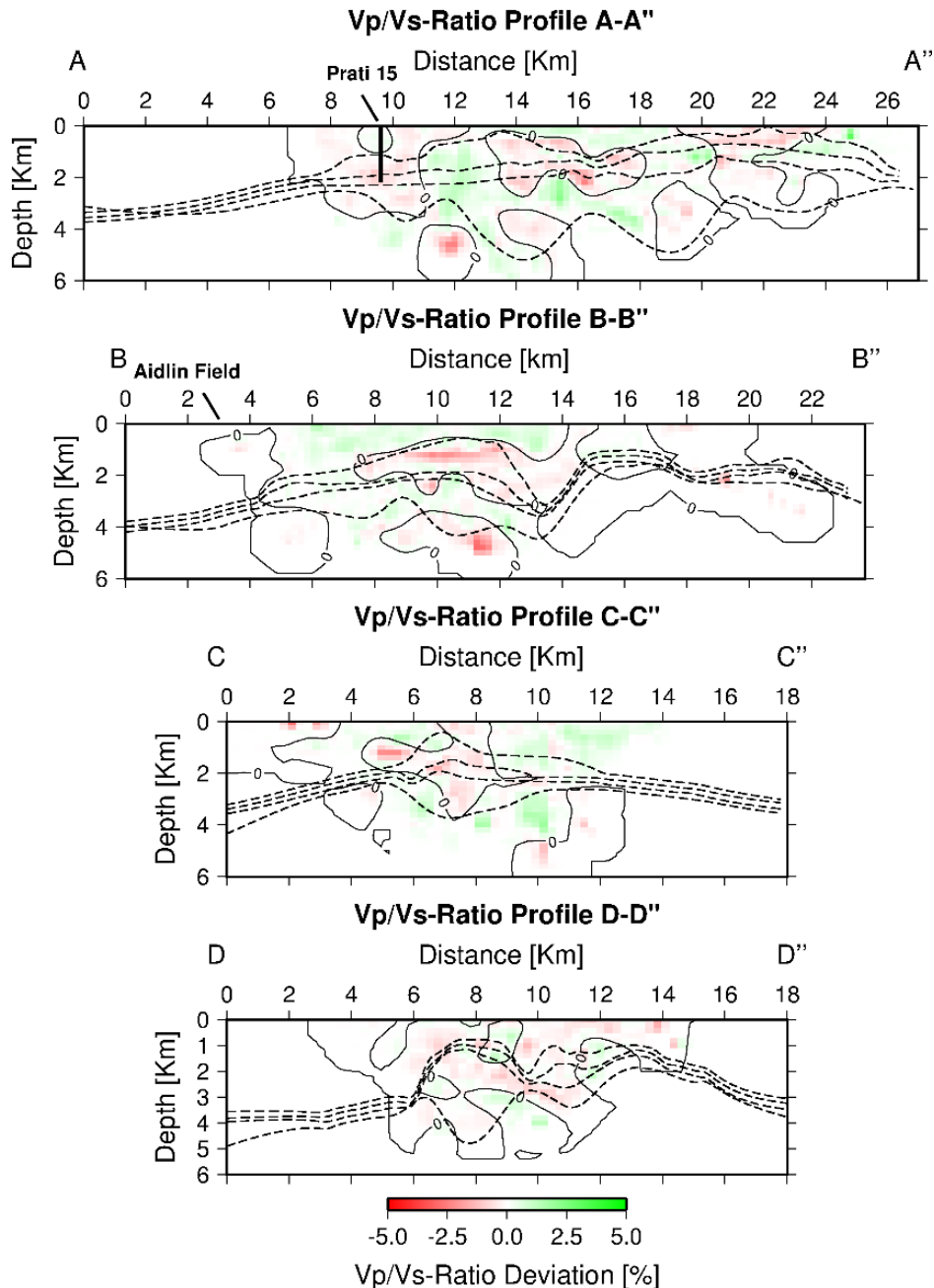


**Horizontal slices of the temporal changes in Vp/Vs when differentiating the 2023 and 2018.2019 results (2023-2018.2019). The results are shown only for regions that have sufficient ray coverage, as determined by the DWS. The outline of the steam reservoir is given by the red polygon, while the surface traces of known faults in the region are shown by the black lines.**

Source: Gritto et al., 2024

The magnitude of change is confirmed by the results in Figure A-4, which displays vertical cross sections along the profiles indicated by the blue lines in Figure A-3. The cross sections reveal how the temporal changes are confined to the upper reservoir and mostly concentrated along profiles A-A'' and B-B.'' The spatial correlation of the temporal changes in Vp/Vs to reservoir operations was addressed in Chapter 3, "Appraising Spatio-Temporal Vp/Vs Results."

**Figure A-4: Vertical Cross Sections of Temporal Changes in Vp/Vs**



Vertical slices through the profiles indicated by the blue lines in Figure A-3. The results represent the temporal changes in Vp/Vs when differentiating the 2023 and 2018.2019 results (2023-2018.2019) and are shown only for regions that have sufficient ray coverage, as determined by the DWS. The dashed lines denote (from top to bottom) the top of the steam reservoir, the top of the hornfelsic graywacke, the top of the felsite intrusion, and the base of the steam reservoir.

Source: Gritto et al., 2024



**CALIFORNIA  
ENERGY COMMISSION**



**ENERGY RESEARCH AND DEVELOPMENT DIVISION**

# **Appendix B: Time-lapse Joint Inversion**

**June 2024 | CEC-500-2024-075**



# APPENDIX B:

## Time-lapse Joint Inversion

---

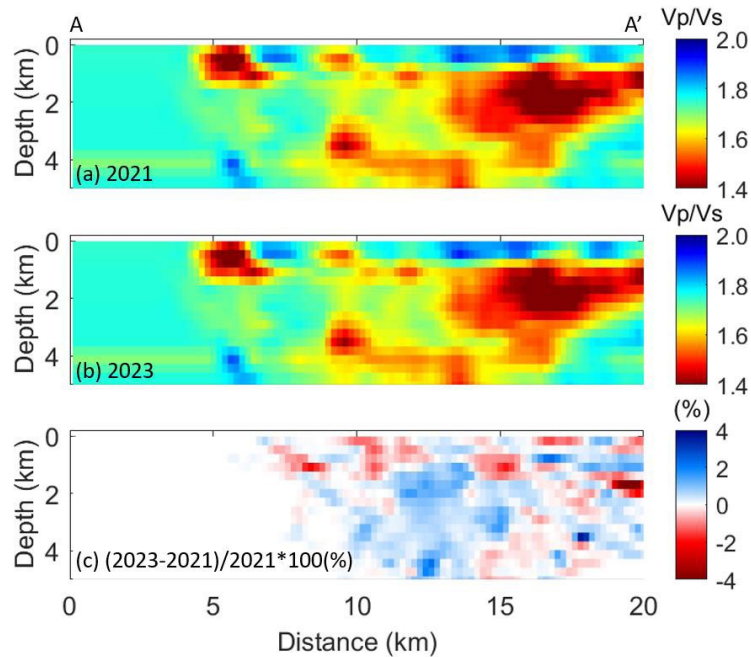
### Time-lapse Single-physics Inversion

The single-physics inversion results for seismic data for 2021 and 2023 are shown below, because they served as a reference for the MT results from the multi-physics inversion results in the section of Chapter 3 titled “Joint Inversion of Multi-physics Data.”

Figure B-1 shows a cross-sectional view of the Vp/Vs model resulting from the inversion of seismic data from the years 2021 and 2023 along profile A-A” (Chapter 3, Figure 14). The figure also illustrates the relative differences between the Vp/Vs models of the two years, providing insight into the detailed changes associated with variations in fluid and steam distribution. To assess the relative difference of the two Vp/Vs models, two separate inversions of seismic data were conducted, based on common events, common damping, and common ray paths (Gritto et al., 2013b). Despite the fact that the relative differences between the two models are fairly small and do not exceed  $\pm 5$  percent, the observed magnitude of change is considered reasonable, considering the two-year timeframe in which these changes occurred.

In contrast, the relative differences between the two MT images exceeded  $\pm 100$  percent. However, the difference plots fell short in providing detailed insights, mainly due to the relatively low resolution of standalone MT images, despite the high sensitivity of MT data to conductive geothermal fluid. For instance, Figure B-2 displays the two single-physics MT inversion images and their relative difference plot along profile A-A.” Due to the inherent low MT resolution, correlating the relative difference plot (Figure B-2c) of the two MT models with that of the corresponding Vp/Vs models (Figure B-1c) becomes nearly impossible. The temporal differences in the MT models are primarily evident in the near-surface, an area that is not the focus of this study.

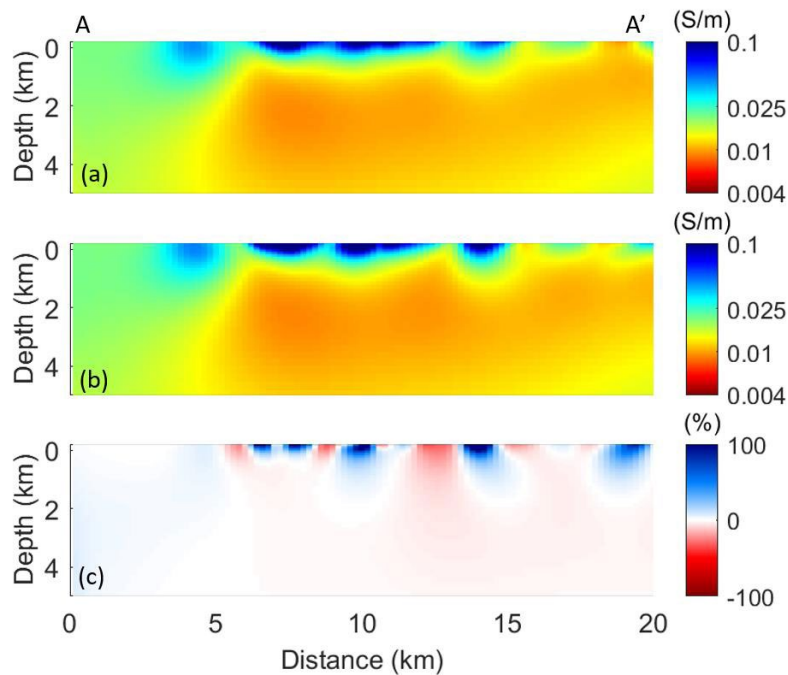
**Figure B-1: Cross Sections of Vp/Vs for Years 2021 and 2023 After Single Inversion**



**Comparison of the Vp/Vs models for the years (a) 2021 and (b) 2023 with (c) corresponding relative differences (expressed as percentages) along Profile A-A'' in Figure 14.**

Source: Gritto et al., 2024

**Figure B-2: Cross Sections of Electrical Conductivity for Years 2021 and 2023 After Single Inversion**



**Comparison of the conductivity models for the years (a) 2021 and (b) 2023 with (c) corresponding relative differences (expressed as percentages) along Profile A-A'' in Figure 14.**

Source: Gritto et al., 2024



**CALIFORNIA  
ENERGY COMMISSION**



**ENERGY RESEARCH AND DEVELOPMENT DIVISION**

# **Appendix C: Geophysical Data Acquisition**

**June 2024 | CEC-500-2024-075**



# APPENDIX C:

## Geophysical Data Acquisition

---

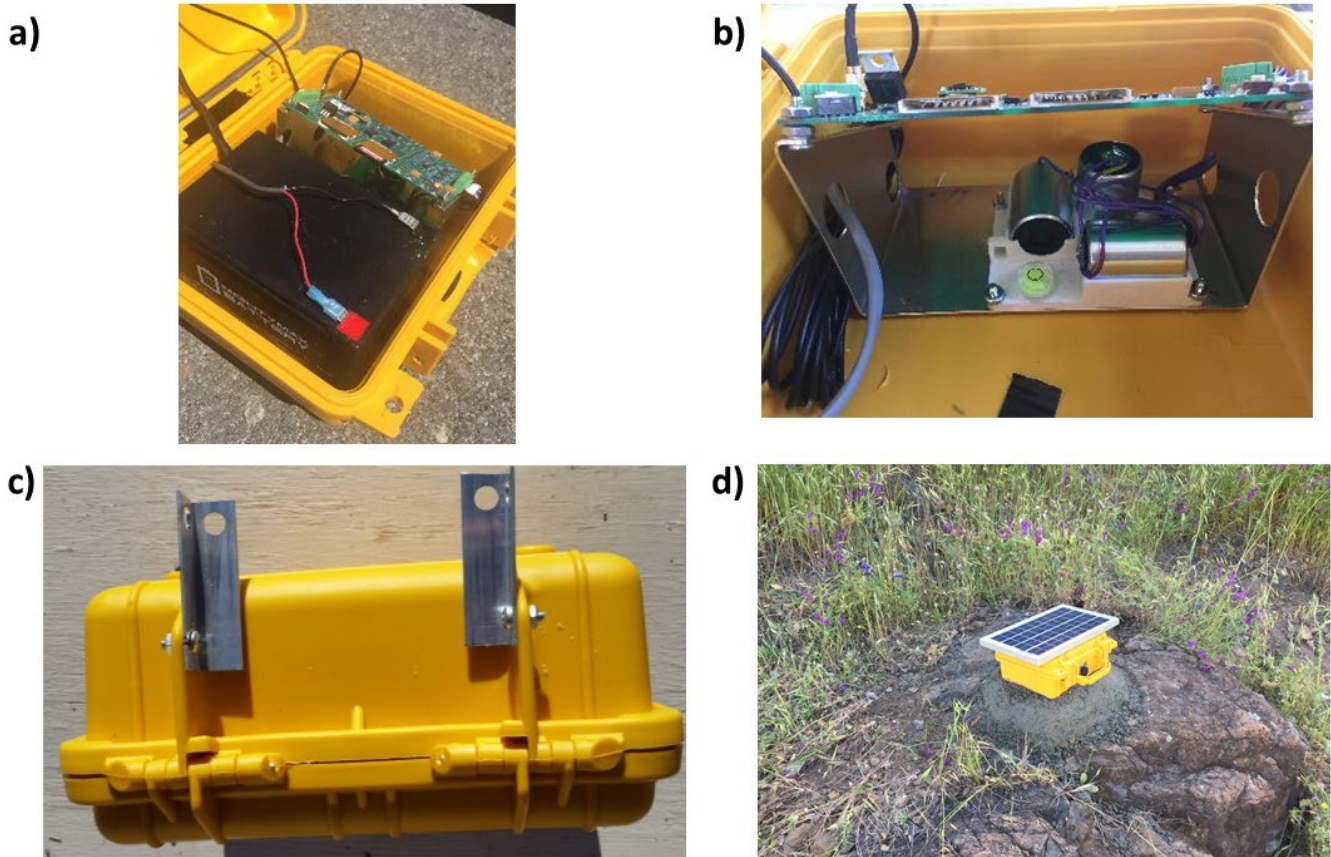
### Seismic Data Acquisition

A map of the combined seismic network currently operating at The Geysers geothermal reservoir was presented in Figure 2, which shows the locations of the temporary CEC-network stations and of the permanent BG-network. While the BG-network covers the entire reservoir, the CEC-network was deployed in the northwest Geysers to support the development of Calpine's operation in this area. The development and deployment of the temporary seismic stations was funded by a recent California Energy Commission project (EPC-16-021, Gritto and Nakagawa, 2020) and the resulting CEC-network was leveraged during the current project.

The design of a CEC-network seismic station and its components is shown in Figure C-1. The 12-volt battery next to the electronic circuit board can be seen in Figure C-1a. At the top of the circuit board, two slots for SD memory cards are visible, as well as the GPS antenna cable. Three orthogonally oriented 4.5-hertz (Hz) geophone components are mounted to the metal bracket below the circuit board (Figure C-1b), while the metal fins are connected to the outside of the enclosure (Figure C-1c) and extend into the concrete pad for improved coupling as shown in Figure C-1d. While the design of the seismic stations includes a mobile phone circuit board for automatic data transmission, the lack of mobile network coverage at The Geysers requires data storage on local SD cards and regular data collection from the CEC-network. The physical properties of the CEC-network stations are summarized in Table C-1.

The permanently deployed BG-network has been in operation for several decades and has been expanded and upgraded multiple times. At present, it comprises 48 surface and shallow borehole stations with 4.5 Hz and 2 Hz three-component sensors. In contrast to the CEC-network stations, data from the BG stations are telemetered to a local computer at a Calpine facility, where the seismic data are preprocessed for event detection and waveforms are formatted. The data are subsequently transmitted to a processing center for further analysis. A picture of a BG surface station is presented in Figure C-2. The components of the stations are mounted on a pole, with a radio antenna for data transmission at the top. The solar panel supplies power for the electronics, which are housed in the gray box below. The box contains two batteries, one GPS unit for time keeping, and a digitizer. The three-component sensor is buried below the surface at the base of the pole. The radio signal of each station is transmitted to a central antenna, from which the data are relayed by a local area network to a computer at a Calpine facility.

**Figure C-1: Temporary Seismic Station Components**



**(a) Interior of a temporary seismic station, with battery and circuit board. (b) Metal bracket with circuit board (top) and three orthogonally oriented geophones (bottom). (c) Metal fins on outside of watertight enclosure for improved coupling to concrete pad. (d) Station installed on a rock outcrop.**

Source: Gritto et al., 2024

**Table C-1: Physical Properties of Temporary Seismic Station**

Property	Value
Size	25x25x10 cm
Weight	4 kg
Input Voltage	10-16 VDC
Solar Panel	10 W, Not Tilting
Power Consumption	360 MW
Sensors	4.5 Hz, HGS, HG6-HS
Data Conversion	24 bit
Number of Channels	3
Sample Rate	200 sps ( $f_{NY} = 100$ Hz)



Property	Value
Time Base	GPS (Internal Antenna)
GPS Accuracy	1 ms
Recording	Continuous
Output	SD Memory Card, 2 slots
Enclosure	Watertight
Coupling	Concrete and Metal Fins

**Figure C-2: Permanent Seismic Station at The Geysers Geothermal Reservoir**



**Site of a permanent seismic station at The Geysers geothermal field with antenna, solar panel, and box housing electronic components. The seismic sensor is buried at the foot of the pole.**

Source: Gritto et al., 2024

Field campaigns to collect passive seismic data recorded by the CEC stations were conducted on a quarterly basis during the duration of the project. Data recovery was quite high, since most temporary stations obtained technical upgrades in December 2020 during the aforementioned CEC project (EPC-16-021, Gritto and Nakagawa, 2020), including new batteries and software upgrades. During each field campaign, the status of the stations was assessed and defective parts were replaced as necessary. Furthermore, batteries were replaced on a regular basis when their capacity decreased below a certain threshold. Figure

C-3 shows the location of a station that was being serviced during a field campaign. Access to this station required a strenuous one-hour return trip down a steep ravine through brush and burnt trees from a recent fire.

**Figure C-3: Temporary Seismic Station at The Geysers Geothermal Reservoir**



**Site visit to a temporary seismic station at The Geysers geothermal field. During each visit SD memory cards were exchanged and the technical status of the stations was assessed.**

Source: Gritto et al., 2024

While the design of the temporary seismic stations was intended for a period of approximately one year, the network is currently operating in its sixth year and does not show signs of deterioration. However, since the original network was established, seven stations were lost to fires, suffered damage by trucks on well pads, or were vandalized. Figure C-4 shows two stations that suffered damage due to a recent fire and to an encounter with a truck on a well pad.

During the last field campaign to collect seismic data, the stations were fitted with SD cards with 64 GB memory, which can record data for a period of approximately one year. This was intended to minimize data loss in case follow-up studies were available in the future.

**Figure C-4: Damaged Temporary Seismic Stations at The Geysers Reservoir**

**a)**



**b)**



**Temporary stations that sustained damage in the field: (a) station destroyed during a recent fire, and (b) station run over by a truck.**

Source: Gritto et al., 2024

## **Magnetotelluric Data Acquisition**

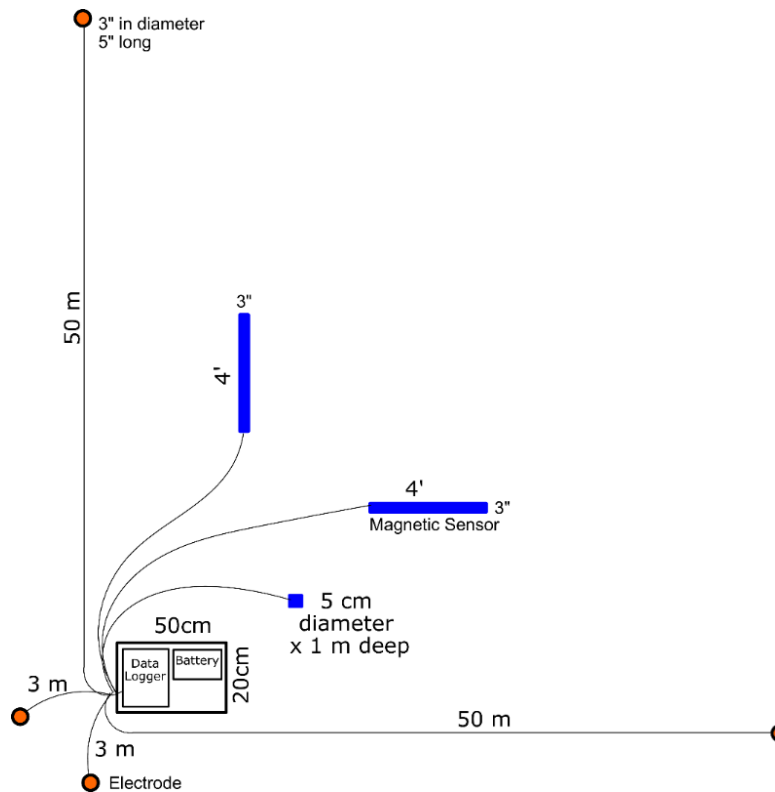
Magnetotellurics is a geophysical electromagnetic method that measures the earth's response to natural time-varying magnetic fields. Following are a few important aspects of MT.

- Unlike wave propagation methods, MT is a diffusive method, meaning the depth is sensitive to the amount of time and frequency you measure at. The MT transfer function is frequency dependent.
- MT is a passive method, meaning the instruments are only listening.
- Electromagnetic waves are polarized; therefore, MT measurements innately include directional information.
- The physical property that MT is sensitive to is electrical resistivity, the inverse of electrical conductivity.

Field measurements are relatively straight forward (Figure C-5). The entire setup is controlled by a data logger shown in the lower left corner in Figure C-5. This is powered by a Li-ion battery that lasts up to three days and is housed in a plastic box for protection from the

weather. The data logger has a GPS antenna and records a time stamp every second for accurate timing.

**Figure C-5: Schematic of a Basic Magnetotelluric Field Station**



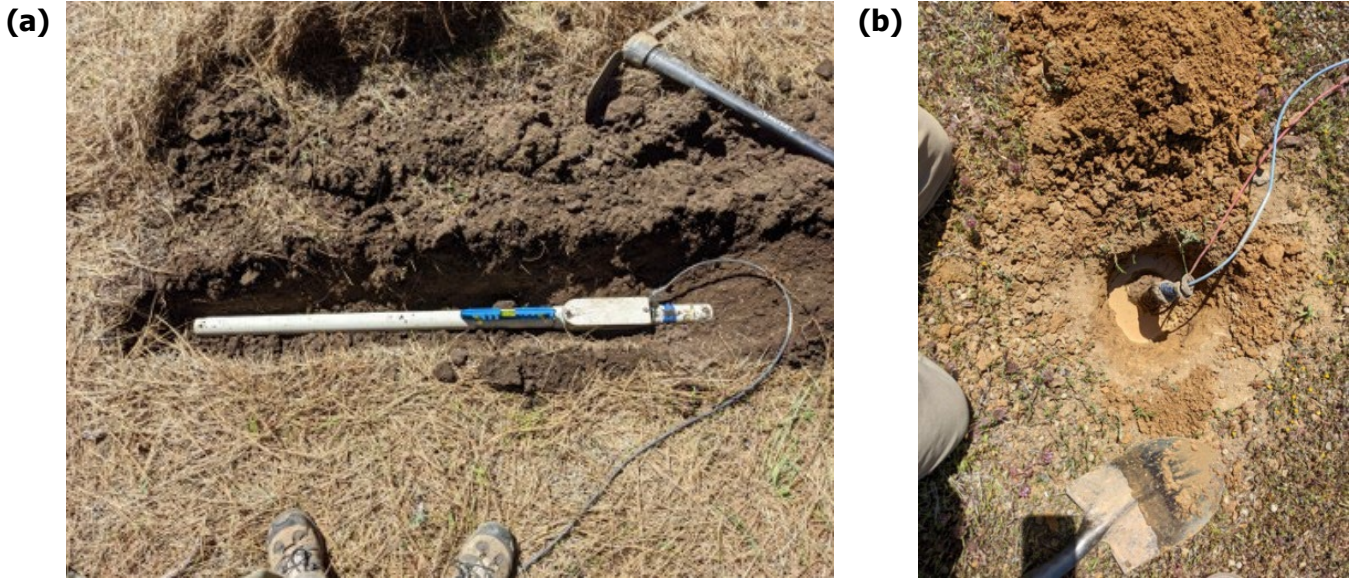
**A schematic of a magnetotelluric field station, with antennas, electrodes, and data logger.**

Source: Gritto et al., 2024

Natural time-varying magnetic fields are measured with magnetic induction coils. These are basically long tubes with thousands of loops of copper wire, and they are buried just below the surface. For The Geysers, the project team measured the horizontal components and did not measure the vertical component because of noise and digging restrictions (Figure C-6a). Electric fields are measured with nonpolarizing electrodes that have a one-way porous bottom and are filled with a solid state copper-copper sulfate mixture (Figure C-6b). These are placed in bags filled with wet clay to get better contact with the ground. Dipoles (a positive and a negative electrode connected by a wire about 50 meters apart) are oriented in north-south and east-west directions. This setup takes about 45 minutes and is left over night for a total of 16–20 hours of data acquisition (Figure C-7). The following day, the station is picked up and moved to the next location. For the current project, the team was able to deploy five stations per day.

The permitting allowed digging on typically old well pads, which resembled parking lots, so the team used pickaxes and digging bars to bury the equipment. With the annual repeats, most holes could be reused from the previous year.

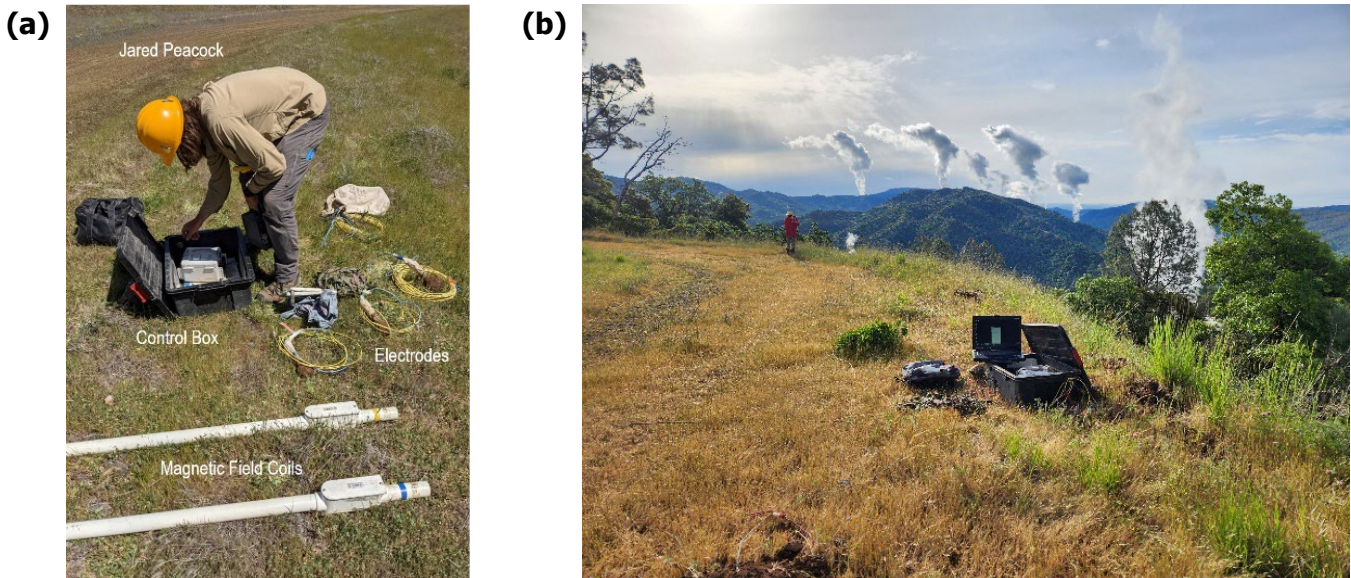
**Figure C-6: Magnetic Field Sensor and Electrodes**



**Installation of magnetotelluric equipment in the field: (a) an antenna measuring the magnetic field, and (b) an electrode measuring the electric field.**

Source: Gritto et al., 2024

**Figure C-7: Magnetotelluric Field Equipment and Data Transfer to a Computer**



**(a) Typical field equipment for a magnetotelluric station. (b) Data acquisition site near the Aidlin power plant in the northwest Geysers looking southward. On a chilly morning, the steam plumes from the active power plants are visible in the distance. In the foreground, a computer is connected to the magnetotelluric data logger for data download.**

Source: Gritto et al., 2024